POLITECNICO DI TORINO

Master's Degree in Nanotechnologies for ICTs

TOWARDS MULTIPEXED BIOSENSING IN FLOW

Supervisors

Dr. Nako NAKATSUKA

Prof. Matteo COCUZZA

Candidate

Fiorella DI SANTO

Academic Year 2021/2022

Abstract

Dopamine is an essential neurotransmitter involved in multiple physiological functions, and altered dopamine levels are implicated in several neurological and psychiatric disorders. A novel technique to functionalize quartz nanopipettes with ca. 10 nm orifice with molecular recognition elements named aptamers is proposed. The dopamine-specific aptamers undergo conformational reorganization upon target binding and recognize dopamine with high specificity and selectivity. Multiple dopamine detection in flow are demonstrated thanks to the reset-ability of aptamers. Furthermore, the specific binding is examined through complementary surface-sensitive techniques, such as quartz crystal microbalance with dissipation and optical waveguide lightmode spectroscopy. In addition, double pore nanopipettes were functionalized with the dopamine aptamer and the control sequence to perform multiplexed measurements within confined spaces. The possibility to execute multiplexed biosensing give the chance to perform self-referenced neurotransmitter monitoring and multiple analytes detection.

Acknowledgements

First of all, I would like to thank my supervisor, Dr. Nako Nakatsuka, and Prof. Janos Vörös for the opportunity to work at LBB and be part of this wonderful research group. Their constant support and insightful suggestions were motivating during the thesis work. I am grateful to Annina Stuber for her precious advice and moral support. My gratitude goes to my supervisor Prof. Matteo Cocuzza for his constant feedback and helpfulness. Then, a special thanks goes to all the LBB members for the amazing working environment and cheerful moments we shared. My special thanks go to the N17 team for the precious and unforgettable moments we spent together. In conclusion, I would also like to show my deep appreciation to my friends and my family for their constant support and encouragement.

Table of Contents

List of Tables

List of Figures

Acronyms

MQW
Milli-Q Water

ICR
Ion-current rectification

DA
Dopamine

AA
Ascorbic acid

PLL-g-PEG
Poly(L-lysine)-graft-poly(ethylene glycol)

SEM
Scanning electron microscopy

TEM
Transmission electron microscopy

PBS
Phosphate-buffered saline

aCSF
Artificial cerebrospinal fluid

Chapter 1

Introduction

Measuring specific chemical interactions with high spatial and temporal resolution to gain insights in neuronal communication is one of today's major challenges. Neuronal communication is a combination of electrical and chemical events. Measuring the electrical activity is limited to neuronal activity and does not enable the tracking of neurotransmitters.

Neurotransmitters are chemicals discovered in 1926 by Otto Loewi which permit neuronal communication throughout the body. These chemicals carry information from one nerve cell to a target cell like a nerve, muscle or gland cell. The nervous system is composed of nerve cells as fundamental units and regulates several body functions such as muscle movements, involuntary processes (*e.g.* heartbeat and hormone regulation), sensory, memory, and learning activities. To regulate all these functions, there are numerous neurotransmitters, such as acetylcholine, glutamate, GABA, glycine, dopamine, norepinephrine, and serotonin.[1][2] A common classification is dividing neurotransmitters as excitatory when they activate cation channels (*e.g.* glutamate and norepinephrine), or inhibitory when anion channels are activated (*e.g.* GABA and serotonin).[1]

Neurotransmitters enable the brain to control these functions through the chemical synaptic transmission that relies primarily on the release of neurotransmitters from presynaptic neural cells to postsynaptic receptors, which are stored within synaptic vesicles at the presynaptic terminal. A nerve cell comprises three main sections: a cell body, an axon where the electrical signal is transported, and an axon terminal where the electrical information is translated to chemical information using neurotransmitters.[1] The axon terminal is also part of chemical synapses, which are the junctions between two nerve cells or between a nerve cell and a non-neuronal cell. They are organized as a presynaptic element (such as a nerve-axon terminal), a postsynaptic site where neurotransmitter receptors are present on dendrites, an extension from the nerve cell body, and a synaptic cleft.[3] Neurotransmitter-specific transporters are placed at the presynaptic terminal, and they inactivate the unbounded neurotransmitters to avoid any high excess concentration in the brain.[2]

Several neurological disorders are correlated to alterations in the levels of specific neurotransmitters. Some of these disorders are Parkinson's disease, schizophrenia, depression, and Alzheimer's disease.[4]

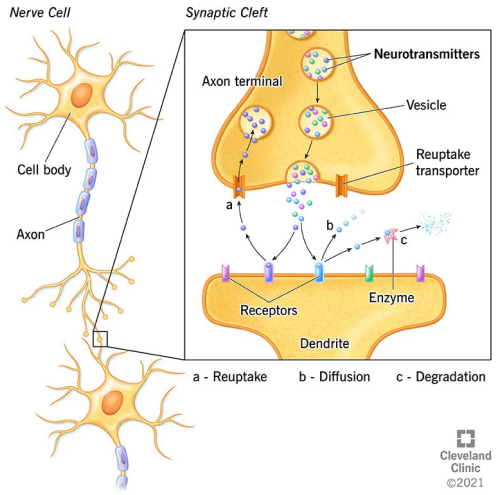

Figure 1.1: Schematic illustration of the synaptic cleft and the role of neurotransmitters.[5]

Dopamine

Dopamine (DA, 3,4-dihydroxy phenylalanine) is an essential neurotransmitter involved in multiple physiological functions, including movement control, modulation of emotional states, cardiovascular, renal, and hormonal systems regulation, reward mechanisms and addiction, attention and memory activities.[6][7][8] Dopamine can be either excitatory or inhibitory depending on which receptors are found on the postsynaptic site; therefore, DA can have different functional roles depending on receptor subtype, cell type and the involved brain region. As a general trend in the nervous system, high dopamine levels indicate cardiotoxicity, addiction and mania, while low levels are implicated in several neurological diseases such as Parkinson's disease, schizophrenia, Alzheimer's disease, stress and depression.[9] The diseases related to dopamine levels could be related to the non-secretion of DA or to dopamine active transporter, which is not regulating the DA level in the brain correctly.

Luisa Speranza *et al.*[7] extensively report how the effect of altered DA levels depends on the brain section. An increase in DA levels is typically related to the motivation and reward mechanisms (*e.g.* sex, food, listening to music and drugs)[8]; however, this molecule could be associated with hyperkinetic disorders (*e.g.* involuntary and sudden movements) or tics when the excess is present in the striatum. If a DA deficiency is present in the same brain region, movement disorders such as stiffness, tremors and slowness of movement can come up. In the hippocampus, the presence of DA is associated with learning, working memory, and long-term memory

formation.[7] Another essential role of DA is in learning and memory, and particularly in memory-related neuroplasticity because of the action of DA on dendritic spines. Therefore, the effect of DA on dendritic spines places this molecule at the interface between the motor and the cognitive systems.[7]

Sujit Basu and Partha Sarathi Dasgupta[10][11] described a possible correlation between brain DA levels and the immune system. Dopamine is one of the important mediators of neuroimmune interactions, and altered immune functions have been observed in diseases like schizophrenia and Parkinson's disease with abnormal dopaminergic systems.[11]

Dysfunction in the dopaminergic transmission is recognized as a core alteration in several devastating neurological and psychiatric disorders. Thus it is of utmost importance to monitor dopamine flux.[9] The normal DA range for a healthy person is from the nanomolar range to the millimolar range, depending on the analyzed brain region. According to the Human Metabolome Database, the physiological DA concentration levels fluctuate in numerous biological fluids, including serum, urine, plasma, cerebral spinal fluid, and platelets. Thus, the sensitive and selective determination of the DA concentration is essential for the understanding of certain disorders that are linked to abnormal levels of DA.[9]

1.1 Existing methods for measuring dopamine

The crucial role of dopamine in the function of the human central nervous system is evident, and the abnormal release of dopamine is linked to neurological and psychiatric diseases. Therefore, accurate sensors capable of monitoring neurotransmitter levels would provide valuable details in neuronal communication through neurotransmitters. Achieving sensitive biosensors with sub-nanomolar limits of detection show significant challenges such as sensitivity, selectivity, and response time.[12] Several techniques have been developed to detect dopamine based on electrochemical and optical readout mechanisms. Existing methods include microdialysis, spectrophotometry, liquid chromatography, chemiluminescence, fluorescence, and molecular recognition techniques.[13] Microdialysis describes the technique of collecting, monitoring and quantifying neurotransmitters in the extracellular environment in the brain and periphery. After the sample is collected, any analytical technique can be used to quantify the target, *e.g.* liquid chromatography and voltammetric measurements, and the detected neurotransmitters are not limited to electroactive analytes.[14] The main disadvantages are the limited time resolution (usually $\geq 1\,\text{min}$), the depleted region of the solutes that can cross the probe membrane during the collecting process, and the tip dimension in the micrometric range.[14]

Electrochemical biosensors take advantage of a specific sensing element which reacts selectively with an electrochemically active target and generates a signal: dopamine contains two phenolic hydroxyl groups which can be easily oxidized, leading to the formation of dopamine-o-quinone on the surface electrodes with an oxidation potential of 150 mV (vs Ag/AgCl).[15][16] Many electrochemical methods have been

developed where a constant or variable voltage is applied, and the current is recorded: amperometry, linear sweep cyclic voltammetry, differential pulse voltammetry and fast-scan cyclic voltammetry (100 times faster than cyclic voltammetry). In amperometry, the current is proportional to the target concentration, while during cyclic voltammetry experiments, the intensity of current peaks gives information about the analyte concentration.[15] The electrochemical biosensing allows performing fast, *in situ* and *in vivo* measurements with high spatial and temporal resolution at low costs, but the interference from species with a similar redox potential (ascorbic acid and uric acid) is the main limitation.[13][15][13][12] Selectivity is essential when real samples are analyzed due to their complexity. Biological samples contain common dopamine interferents, but also other neurotransmitters and molecules. To overcome the selectivity issue and to increase the sensitivity, the deposition of nanomaterials and nanostructures have been developed to coat the surface's electrodes: metal nanomaterials (*e.g.* gold nanostructures and palladium nanoparticles), carbon nanomaterials (graphene and carbon nanotubes), and polymers (conducting polymers and molecularly imprinted polymers, *e.g.* polypyrrole and PEDOT:PSS), which can all improve the electrocatalytic oxidation of dopamine.[15][16][12] With these electrodes' modifications, the achieved detection limit is in the picomolar range, but one limitation is the spatial resolution due to the electrodes' dimensions in the micrometric range.

Several biosensors based on biological molecules for target recognition, such as enzymes, antibodies, and aptamers, have been developed to detect dopamine. Biosensors based on molecular recognition methods are applied to optical and electrochemical read-out mechanisms. Enzymes show high catalytic efficiency and specificity for small molecule detection; developed enzymes for dopamine are polyphenol oxidase, tyramine oxidase, laccase, and tyrosinase.[13] For example, a chemiluminescence enzyme-based biosensor with a limit of detection of 10 nM was developed where H_2O_2 was produced during the dopamine oxidation by tyramine oxidase, and the luminol reacted with the produced H_2O_2 to generate chemiluminescence.[13] However, dopamine is an electroactive molecule that can be easily oxidized without an enzyme, and enzymes are difficult to purify, less stable, and have complex immobilization processes.[13] Antibodies show high binding affinity, greater specificity, and mature detection platforms such as ELISA and lateral flow devices. A dopamine antibody was immobilized on gold nanoparticles, and the dopamine concentration was measured as a variation in the localized surface plasmon resonance.[13] Several fluorescent aptamer-based biosensors using traditional fluorophores and quantum dots were reported. A fluorophore-labelled aptamer is linked to quenching nanomaterials, and enhanced fluorescence is measured when dopamine bonds to aptamers.[13] Aptamers show versatile signal transduction mechanisms, fast response time, high stability, low cost and easy modification compared to antibodies.[13]

Electrolyte-Gated Organic[17] and aptamer-based[18] field-effect transistors are tools to monitor neurotransmitters *in vitro* and *in vivo*. The dopamine detection tunes capacitance and threshold voltage with a limit of detection up to the picomolar scale. Easy and matured fabrication protocol, real-time measurements are the major

advantages.[17]

The optical read-out mechanism includes liquid chromatography, gas chromatography, colorimetry, fluorimetry, electrophoresis, and electrochemiluminescence. [13] Long analysis times, the requirement of sophisticated instrumentation, high cost, and pre-treatment of the sample during analysis are some drawbacks related to optical read-out techniques.[19][13] The simultaneous detection of dopamine in the presence of several interfering molecules remains a fundamental challenge even for optical-based technique, even if sub-picomolar concentration can be achieved as the limit of detection.

All the above-described techniques show some limitations: the selectivity when interfering molecules are present, real-time response and spatial resolution. Aptamer-based biosensors can address the selectivity issue, and developing aptamer-modified nanopipettes enable highly sensitive measurements with precise spatial resolution.

1.2 Aptamer-modified nanopipettes

The term nanopipette describes a glass or quartz pipette with an aperture smaller than 200 nm with a needle-like tip.[20] Pre-pulled glass or quartz nanopipettes, including bare and chemically modified nanopipettes, have been employed in resistive-pulse, rectification and electrochemical sensing.[21] Real-time biological process monitoring, chemical ion sensing, and single entity analysis are the primary applications.[22] The ease of fabrication and the needle-like geometry with nanometer-sized tips make them suitable for local measurements and nanoparticle delivery in restricted spaces. Further, nanopipettes are convenient for scanning probe microscopies, including scanning ion conductance microscopy (SICM) and scanning electrochemical microscopy (SECM).[22]

The nanometric aperture allows nanopipettes to be used for resistive pulse detection and current rectification sensing which are based on the translocation of molecules through the opening.[21] In resistive-pulse sensing a momentary drop in the base current when the analyte translocates through the aperture generates a current pulse.[23] The spike in current can be used to detect the molecule[21], while analyzing the magnitude and shape of the current pulses reveals information about the size, shape or charge of the analyte.[23] The resistive-pulse technique is used to analyze DNA detection and sequencing, particle separation and single-cell.[21]

The ion current rectification (ICR) is described as the asymmetry of the current-voltage response: the ion current at one potential polarity is much higher than at the opposite polarity at the same voltage magnitude.[22] The ICR can be modified by chemical functionalization or the binding of analytes on the inner walls, as well as the ion concentration and pH of the solution used inside the pipette and in the external bath. The rectification has been observed only when the aperture of the nanopipette is comparable to the diffuse double layer.[20] This technique allows the

sensing of ions and molecules of interest and can be easily evaluated through the cyclic voltammetry (CV) method.

Both techniques are dependent on the geometry of the tip. The inner wall is chemically modified to increase the selectivity of the pre-pulled nanopipettes to selective analytes in resistive pulse sensing and ICR. Aptamers and nanoparticles are common functionalization elements.[20][22]

Resistive pulse and current rectification sensing are the main applications, but nanopipettes can be filled with conductive materials to provide electrochemical sensing.[22] Further, the geometry of the tip of nanopipettes makes them suitable to penetrate cells without damaging them.[23] The main drawback of nanopipettes is the lack of geometry reproducibility. Improving the fabrication reproducibility and lowering the cost of characterization could even expand the applications. Among all the different types of nanopores, quartz nanopipettes show ease of fabrication, needle-like structure, and a wide range of possible modifications to create different functional probes and they are suitable for detection of single molecules without labelling in low-volume samples.[23][22]

A double pore nanopipette is obtained from a capillary with two pores separated through a barrel of the same material of the capillary. One advantage of double pore nanopipettes instead of two single pore ones placed close to each other is the possibility to perform the detections in the exact same environment. Given the density and complexity of brain tissues, even a micrometric distance between the two nanopipettes would lead to different environments and analyte concentrations. Functionalizing selectively the two pores with two different aptamers would lead to the development of a multiplexed biosensors with the possibility to have a sensor pore and a control pore or two sensor pores to detect two different analytes.

Aptamers

Aptamers are short (typically between 20 and 80 nucleotides with 6–30 kDa molecular weights[24][25]) single-stranded oligonucleotides (*e.g.* RNA, DNA, and modified oligonucleotides) with unique binding properties. Aptamers bind to target molecules with high specificity and affinity through van der Waals forces, hydrogen bonding, electrostatic interactions, and shape complementarity.[25] A large number of aptamers have been identified against different targets, including small organics, peptides, proteins[26], whole cells, large protein complexes[24] and drugs[25].

The binding affinities depend on the target in the range from the picomolar scale to the nanomolar scale for several proteins: higher affinity could lead to lower limits of detection. The selectivity enables aptamers to distinguish similarly structured molecules. When binding to the target molecule, some aptamers undergo significant conformational changes that can be analyzed optically and electrochemically.[26][25] The performance of aptamers varies depending on the buffer since they are sensitive

to the type and concentrations of monovalent and divalent cations.[26]

Aptamers can find applications in several aspects: in vitro and in vivo diagnosis, drug release, targeted therapy, biosensors, molecular imaging, and purification of target molecules.[25][27][24] In 2004 the first aptamer-based therapeutic (Macugen) was approved by the US Food and Drug Administration for the treatment of age-related macular degeneration.[27]

The visualization of aptamers' binding can be optical, electrochemical, or mass based.[26] One, or multiple, organic fluorophores can be introduced into the aptamer structure to visualize the binding with a change in fluorescence characteristics in terms of intensity and anisotropy. Depending on the application, quantum dots for monitoring biological systems in real-time and gold nanoparticles for their non-toxic nature can be inserted into the aptamer chain.[26] Electrochemical techniques show simple and low-cost instrumentation with high sensitivity; the main methods are electrochemical impedance spectroscopy (EIS), cyclic voltammetry (CV), and amperometry. In mass-sensitive detection techniques, the detection is performed on a surface where aptamers have been captured and is typically label-free. The most common methods are surface plasmon resonance (SPR), surface acoustic wave (SAW), quartz crystal microbalance (QCM), and microchannel cantilever sensors.[26] These techniques are all based on differential changes in mass to determine aptamers' properties and, besides, they can be applied to the analysis of small molecules such as dopamine and serotonin.[28]

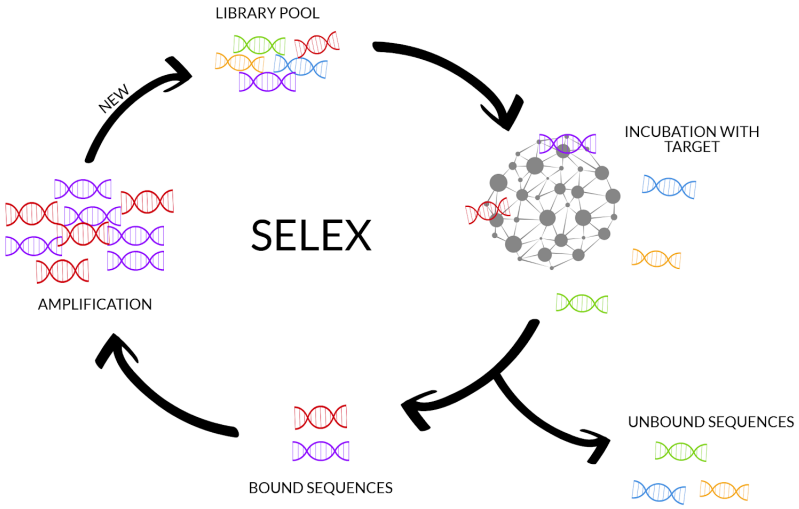

Figure 1.2: Schematic illustration of SELEX protocol for aptamer identification and production.[29]

Systematic Evolution of Ligands by Exponential Enrichment (SELEX) is a standard process used to develop specific aptamers. Multiple rounds of selection and amplification are used to obtain specific aptamers. In the first step, the target

molecule is incubated in a pool of 10^{14}-10^{16} random single-stranded oligonucleotides with a fixed sequence on both ends; then, a filtration between bound and unbound oligonucleotides is performed. Subsequently, the bound oligonucleotides are amplified by the polymerase chain reaction. These three steps are repeated several times depending on the purification level required (Fig.1.2). This standard protocol is not always effective for *in vivo* applications because the binding conformation obtained *in vitro* is different if the isolation buffer is not the same. To overcome this issue, several variations to the standard SELEX technology have been developed, including Cell-SELEX and in vivo SELEX.[25][24]

Aptamers *vs.* Antibodies

Antibodies provide molecular identification, and they are applied in disease diagnosis and therapy. Antibodies have been used for decades and have led to the improvement of diagnostic assays.[24]

Although a similar binding mechanism, aptamers represent a cost-effective, highly consistent, low immunogenicity, non-toxic and highly stable alternative to antibodies.[27][25]

Compared to antibodies, aptamers show better target discrimination and specificity; further, aptamers can penetrate tissue barriers and are not recognized by the immune system enhancing their therapeutic properties. A few other advantages of aptamers are the stability over temperature fluctuations which eases transport and storage, minimal bath-to-batch variation thanks to the chemical synthesis, and the possibility to be developed against a broad range of targets.[25][30] Aptamers could enlarge their applications thanks to low-cost production and easy storage protocols.[30] The main differences between aptamers and antibodies are summarized in Table 1.1.

Aptamer commercialization is still far from the one of antibodies even if aptamers show great advantages. The main hypothesis behind the non spreading of aptamers are the familiarity with the antibodies and the financial investments already made by pharmaceutical and biotech companies in antibodies. One technical limit of aptamers is given by the restricted number of those that bind properly to small molecules.[24]

	Aptamers	**Antibodies**
Molecular weight	$\sim 6 - 30\,\text{kDa}$	$\sim$150$-$180 kDa
Generation time	Few hours to months	Several months
Batches variations	Low	High
Specificity	Higher	Lower
Minimal target size	$\sim 60\,\text{Da}$	$\sim 600\,\text{Da}$
Targets	Wide range of targets	Immunogenic molecules
Chemical modifications	Various modifications	Limited modifications
Stability	Very stable	Temperature and pH
Cost	Lower	Higher
Working conditions	Selected buffer	Physiological conditions
Tissue penetration	Possible	Not possible

Table 1.1: Comparison between aptamers and antibodies. Adapted from [24]

Chapter 2

Experimental methods

Materials

Sigma-Aldrich Chemie GmbH (Buchs, Switzerland) is the main supplier for all chemicals unless otherwise noted. Phosphate-buffered saline at 1× concentration (137 mM NaCl, 2.7 mM KCl, 10 mM Na_2HPO_4, 1.8 mM KH_2PO_4) and pH 7.4 (Thermo Fisher Scientific AG, Reinach, Switzerland) was used as received for all measurements and it was stored at ambient temperature. All solutions were prepared using deionized water with a resistivity of 18.2 $M\Omega\,m^{-1}$ produced by a Milli-Q system (Millipore, Billerica, MA). All DNA solutions (100 µM) were high performance liquid chromatography (HPLC)−purified, aliquoted, and stored at −20 °C until use.[31]

Aptamers

Both thiolated and biotinylated dopamine aptamers have been purchased from Microsynth AG (Balgach, Switzerland). Thiolated single-stranded dopamine aptamer sequence is: (5′/Thiol/CGA CGC CAG TTT GAA GGT TCG TTC GCA GGT GTG GAG TGA CGT CG 3′) with melting point 74 °C, molecular weight 13 969.8 $g\,mol^{-1}$ and thiolated scrambled sequence is: (5′/Thiol/AGT ACG TCG ATG CTC GAT CAG TGG GCT AGG TGC GTA GCG GTC TG 3′) with melting point 73.7 °C, molecular weight 13 871.8 $g\,mol^{-1}$.[32] Biotinylated single-stranded dopamine aptamer sequence is: (5′/Biotin/CGA CGC CAG TTT GAA GGT TCG TTC GCA GGT GTG GAG TGA CGT CG 3′) with melting point 73.7 °C, molecular weight 14 080.8 $g\,mol^{-1}$ and biotinylated scrambled sequence is: (5′/Biotin/AGT ACG TCG ATG CTC GAT CAG TGG GCT AGG TGC GTA GCG GTC TG 3′) with melting point 73.7 °C, molecular weight 14 087.3 $g\,mol^{-1}$.

Nanopipette Fabrication

Single pore nanopipettes were pulled from quartz capillaries (o.d., 1 mm; i.d., 0.5 mm; Friedrich & Dimmock) using a laser puller (P2000, Sutter Instruments). Double

pore nanopipettes dimensions were 1.2 mm of outer diameter and 0.9 mm of inner diameter. The septum of the theta nanopipettes is oriented parallel to the laser beam to ensure a similar pore size. To achieve this the septum was aligned to the ground. The puller was heated at least 30 min before use and the applied parameters to obtain a ~ 10 nm pore were:

- Single pore nanopipettes: (Line 1) Heat 750, Filament 4, Velocity 40, Delay 150, Pull 80; (Line 2) Heat 700, Filament 3, Velocity 60, Delay 135, Pull 180
- Double pore nanopipettes: line 1) Heat 850, Filament 4, Velocity 30, Delay 145, and Pull 110; (line 2) Heat 865, Filament 3, Velocity 20, Delay 135, Pull 170.[32]

The size of the orifice tip is determined mainly by the heat of the laser and applied force to divide the quartz capillary.

Aptamer Functionalization

Silane based functionalization protocol

A three-step functionalization procedure was implemented to immobilize DNA inside the nanopipette.[31] The first phase of the protocol requires the deposition of a single (3-aminopropyl)-trimethoxysilane (APTMS) layer via vapour-phase deposition at 40 °C for 1 h to obtain amine-terminated silanes on the surface of the nanopipette. Then, the nanopipettes were filled with 1 mM solution of 3-maleimidobenzoic acid N-hydroxysuccinimide ester (MBS) dissolved in a 1:9 (v/v) mixture of dimethyl sulfoxide and PBS for 1 h. In this step MicroFil syringe tips (World Precision Instruments, Sarasota, FL) were used to fill the pores of nanopipettes. MBS enables the cross-link between the previously deposited amine-terminated silanes and the thiolated DNA aptamers. The last step involves the incubation of the aptamer solution inside the nanopipettes at room temperature for at least 2 h to overnight; before the incubation, a washing step with PBS was performed. Aptamers were prepared by heating them to room temperature and, then, mixed with 50-fold excess tris(2–carboxyethyl) phosphine (TCEP) for 1 h at room temperature in dark light to reduce the disulfide bonds. Next, the aptamers and TCEP solution was diluted with PBS to reduce the aptamer concentration to 5 µM and cleaned with Zeba spin desalting columns (7K MWCO, 0.5 mL, Thermo Fisher Scientific AG, Reinach, Switzerland); aptamer solution was desalted to eliminate unreacted TCEP that leads to a reduction of the coupling yield due to the reaction of the protecting thiolated group of aptamers to the surface. Before the cleaning step, the spin desalting column is prepared by 3 washing steps with MQW at $1.5\,\mathrm{k}\,rev\ min^{-1}$ for 2 min. Aptamer solution was denatured at 95 °C for 5 min and then cooled down to room temperature before filling the nanopipettes. After the incubation time, the nanopipettes were rinsed in PBS before experimental use.[28]

During the functionalization procedure and the measurements, the nanopipettes were stored in petri dishes and the nanopipettes were immobilized thanks to Blu-Tack from Bostik.

Alternative functionalization protocol

The bare unfunctionalized nanopipettes were incubated with a PLL(20)-g[3.5]-PEG(2)/PEG(3.4)-biotin(15%) solution with a 19.285 µM concentration for $15-20$ min stored at -20 °C. The polymeric solution was heated up to room temperature before the incubation. After the incubation time, the nanopipettes were washed three times with a 1x PBS solution. The aptamers presents a biotinylated group to bind to steptavidin, but the nucleotides chain is the same as in the standard functionalization protocol. Aptamers were denaturated at 95 °C for 5 min, cooled down to room temperature and incubated with a streptavidin solution for $20-30$ min: a molecule ratio of 2 : 1 between aptamers and streptavidin was kept to bind in average half of the free spots of streptavidin. Then this pre-incubated solution was left in the nanopipettes for at least 30 min. After this last step, the nanopipettes were washed again three times with 1x PBS solution.

Measurement set-ups

The current between two Ag/AgCl quasi-reference counter electrodes was measured: one electrode was placed inside the pore of the nanopipette, for theta nanopipette the wire was positioned in the pore to be measured, and the other one in the bulk solution where the nanopipette was immersed. The voltage was applied to the electrode in the bulk solution and the one in the nanopipette was recording the response. The electrode was connected to a variable gain low noise current amplifier (DLPCA-200, FEMTO Messtechnik GmbH, Germany).

A custom-written LabVIEW interface (2017, National Instruments) was used to perform the recording of data, based on the WEC-SPM package provided by Warwick Electrochemistry and Interfaces Group, led by Prof. Unwin. Data collection was carried out by an FPGA card PCIe-7852R (National Instruments).

With the described electrode arrangement two different measurement set-ups were used: manual bath exchange and in-flow recording. In the manual bath exchange set-up, the bath underneath the nanopipette was simply changed with a new bath solution. With the in-flow set-up, the nanopipette and the reference electrode were placed in a Polydimethylsiloxane (PDMS) mold. A pump was pushing the new solution and removing the current solution via an inlet and outlet in the mold. The injection speed was adjusted up to 200 $\mu L\,s^{-1}$: a common applied speed was 20 $\mu L\,s^{-1}$. At each injection 2 mL solution was pumped. To perform a complete solution exchange (*e.g.* from dopamine to PBS) multiple injections were necessary. The pump allows to perform real-time analysis of dopamine detection and mimic real experiments.

Bath solutions

A solution with 100 µM concentration of the target molecule was adopted to characterize the sensors; this saturated concentration is high enough to bind all the

aptamers in the sensing area. In the case of dopamine sensors, adding a 10% of ascorbic acid in the solution avoids the polymerization of dopamine; polymerized dopamine is not recognized by the sensors and acts as a coating to the nanopipette. Dopamine polymerization starts with a first oxidation step where dopamine is oxidized by oxygen to obtain dopamine quinone, then oxidized/rearranged into different quinone structures and followed by a polymerization step.[33] The dopamine polymerization kinetics can be drastically slowed with the addition of ascorbic acid, or also sodium ascorbate: with just a 5% addiction in the solution the polymerization can be stopped for 24 h.[34] The main agents that participate in the polymerization are oxygen, solution pH and UV light. Ascorbic acid has an inhibition effect at acid and basic pHs and it is not affecting the pH of the solution. The ascorbic acid effect is related to the reduction of dopamine quinone by ascorbic acid that compensates for the dopamine oxidation by oxygen. UV light exposure can accelerate the polymerization of dopamine[34][33], so it would be preferable to keep the solution in a dark environment.

Real-Time Measurement

The current-time recordings were monitored while a constant voltage difference of 0.5 V was applied between the bath electrode and the sensing electrode. The noise level was dependent on the electrodes, the environment, the grounding of the system and the single nanopipette behaviour.

Cyclic Voltammetry (CV)

Cyclic voltammetric measurements consists of two ramp functions to repeatedly increase and afterward decrease the voltage in the range between −0.5 V and 0.5 V or −0.7 V and 0.3 V. The scan rate was $0.2\,\mathrm{V\,s^{-1}}$ and CVs were performed to characterize the nanopipettes in terms of rectification factor and current limits. CVs were run before and after real-time measurements to stabilize the current. Running CVs helps in the unbinding of dopamine molecules from the aptamers to go back to the initial current baseline. This allows re-using the sensors for multiple measurements and over time. The number of executed CVs depends on the stability of the measurement: at least 20 CVs were performed in each solution bath, but this number could increase if the current limits at −0.5 V and 0.5 V was not stable.

Data analysis

Real-time recordings were filtered with a Butterworth lowpass filter of the fifth order. Then a digital filter was applied forward and backwards to the signal. The combined filter has zero phase and a filter order twice that of the original. Data are reported as mean ± standard error of the mean.

DNA translocation experiments

The aptamer translocation experiments through a nanopipette were performed with a real-time current analysis where the peaks were visualized in the current response. The current was measured with Ag/AgCl electrodes placed in the nanopipette and in the bath by the application of a voltage difference between these electrodes. The voltage difference range applied was from 0 V to ±2 V: a positive voltage was applied at the nanopipette electrode when the aptamer transversed from the bath to inside the nanopipette and a negative voltage for the opposite direction. The stock aptamer solution was denatured at 95 °C for 5 min and then cooled down to room temperature before diluting to reach 5 µM concentration with PBS. The aptamer solution was used as a bath underneath the nanopipette and inside the nanopipette during different experiments. Quartz and aminosilaned nanopipettes were used during the experiments.

QCM-D

The Q-Sense E4 (Biolin Scientific) with four flow modules was used for the measurements. The resonance frequency, f, and the energy dissipation of the quartz crystal, D, were measured at the fundamental resonance frequency (5 MHz). The third, fifth, seventh, ninth and eleventh overtones were recorded at the same time.

QCM-D chips are coated with a SiO_2 layer. The cleaning process consisted of 3 min in the sonicator sequentially with acetone, isopropanol and MQW. Then, the chip was inserted in the UV Ozone cleaner for 15 min and subsequently, assembled in the holder. Frequency saturation with the examined analyte was reached before rinsing with PBS and inserting a new analyte solution.

The QCM-D data were modelled using Q-tools software 3.1.29. In the viscoelastic Voigt model the 3^{rd}, 5^{th}, 7^{th}, 9^{th} overtones are used to extract mass and thickness of the layer-by-layer functionalization stack. The data were fitted using one layer and the fitting was divided firstly for PLL-g-PEG and, then, for the streptavidin-aptamer complex. The bulk solution (PBS) density and viscosity were assumed to be fixed at $1\,000\,\mathrm{kg\,m^{-3}}$ and $0.001\,\mathrm{kg\,m^{-1}\,s^{-1}}$. The density of the layer was kept fixed at the bulk solution value since it was considered a high hydrated layer ($1\,000\,\mathrm{kg\,m^{-3}}$). The viscosity, shear, and thickness were the parameters to fit with the Voigt model and these parameters were kept within the following boundaries:

	Min-Max estimations	**Steps**
Layer viscosity	$0.000\,5 - 0.01\,\mathrm{kg\,m^{-1}\,s^{-1}}$	5
Layer shear	$10^4 - 10^8\,\mathrm{Pa}$	8
Layer thickness	$10^{-10} - 10^{-6}\,\mathrm{m}$	10000

Table 2.1: Settings to the parameters to be fitted with the Voigt model in QTools

OWLS

The optical sensor chips made of $SiO_2 - TiO_2$ underwent a 15 min cleaning process in the UV Ozone before assembling the chip in the flow cell. An overnight baseline in the buffer solution was necessary before starting the injections. Before washing with PBS or injecting a new solution, the mass saturation was reached for the previous layers.

Chapter 3

Fabrication and characterization of quartz nanopipettes

3.1 Fabrication

P-2000 by Sutter Instrument Co. is a commonly used laser puller to produce nanopipettes. Five parameters control the physical properties of the fabricated nanopipettes: HEAT, FILAMENT, VELOCITY, DELAY, and PULL. The puller is highly affected by the environment: heat and humidity can affect the pore geometry and the same set of parameters can produce different results on other machines or throughout various run cycles.[20] Multi-line programs can allow the production of replicable nanopipettes on the same machine over time.[35] The puller follows a protocol of sequential heating and pulling[20] and the adopted steps are showed in Fig.3.1.

The HEAT parameter determines the laser output power. FILAMENT defines the scanning patter of the laser beam. VELOCITY defines the puller bar's speed before the hard pull. DELAY is the time period between the shut-down of the laser and the start of the hard pull. PULL specifies the force applied during the hard pull. By increasing the value of HEAT, VELOCITY or PULL parameters smaller apertures can be obtained, but the same trend can be obtained by decreasing the value of FILAMENT or DELAY.[21]

A second, and less popular, approach for nanopipette fabrication is the chemical etching method.[23] A micrometer-sized glass pipette is pulled and the tip is fused to be completely closed. Then, the tip is etched in a hydrofluoric acid solution which leads to the formation of an aperture. This technique is more time consuming and the aperture dimension cannot be precisely controlled.[36]

Micropipettes are typically fabricated from borosilicate capillaries, while nanopipettes

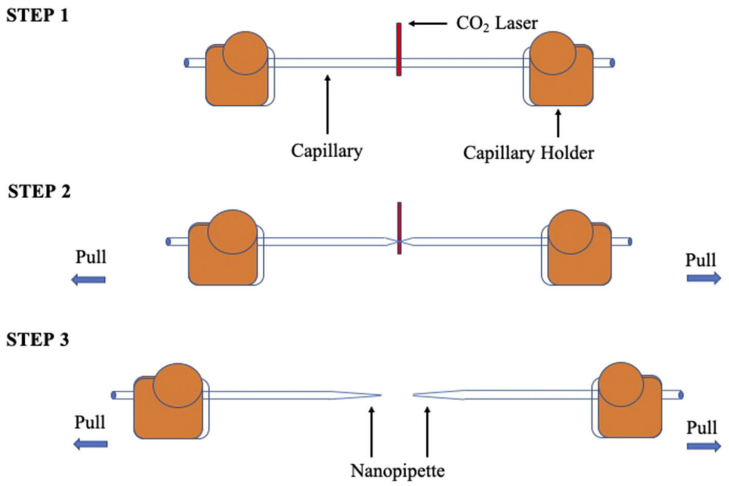

Figure 3.1: Schematic representation of the steps involved in the fabrication of the nanopipette using the laser pipette puller.[20].

are made from quartz.[35] Borosilicate glass shows a lower melting point and lower rigidity than quartz, but this material is unsuitable to produce nanometric apertures. Quartz is sensitive to uneven heating that could result in two asymmetric pulled pipettes from the same capillary.[21] Quartz is suited to be used in single cells and electrochemical applications due to its high mechanical strength and low electrical noise.[20] The material is one of the influencing parameters in the fabrication of nanopipettes, other crucial specifications are the ratio of the outer diameter (OD) to the inner diameter (ID), which determines the aperture's dimension, the thickness of the capillary walls, and the presence or absence of a filament.[22][21]

3.2 Current rectification

The ion-current rectification (ICR) is described as the asymmetry of the current-voltage response. The ion current measured at one voltage polarity (+V) is higher than at the opposite polarity (-V) when the applied voltages have the same magnitude.[37][22] This behaviour highlights the presence of a preferential flow direction that originated from electrostatic interactions between the ions passing through the nanometric-sized opening, and the pore walls.[37][38][21] The rectification has been observed for asymmetrically shaped, *e.g.* cone-shaped, quartz nanopipettes[38] and nanopores that show an aperture's dimension comparable to the diffuse double layer[20] with an excess of surface charge.[37] The ICR can be observed in several nanoporous systems such as nanopores in polymer films and silicon nitride, gold nanotubes[37], and glass capillaries[38].

The electrical double layer develops at the interface between the quartz surface and an electrolyte solution because the counter ions present in the solution are

attracted by the charged surface.[38][23] When the electrical double layer is in the same dimension range of the aperture, the ion flux passes through this charged layer and the ion transport properties are modified by this electrostatic interaction. The transport is not affected when the electrical double layer is negligible with respect to the tip's dimension; this effect can be observed in apertures smaller than 20 nm.[38]

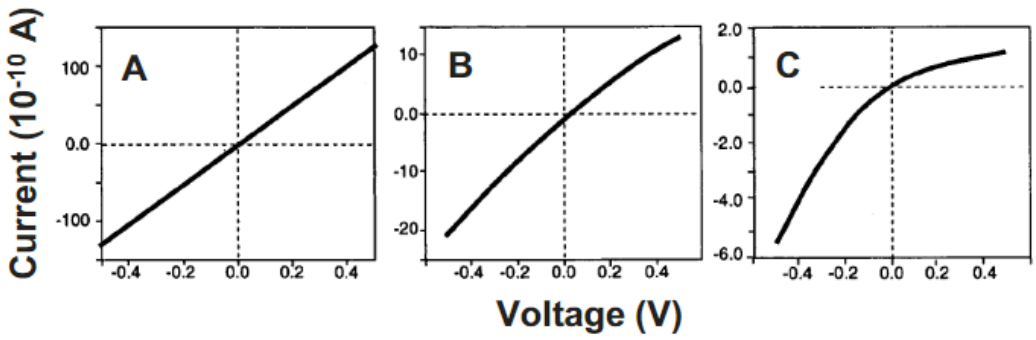

Figure 3.2: Current-voltage curves of a nanopipette of radius ~ 20 nm at A) 1 M KCl, B) 0.1 M KCl, and C) 0.01 M KCl. Measurements were performed at a scan rate of 20 mV s^{-1}. Reprinted from [38][37].

The sign of the surface charge determines the direction of the ICR: positive and negatively charged nanopipettes rectify in opposite directions.[37] In Fig.3.2, Siwy[37] and Wei *et al.*[38] analysed how the pH and electrolyte concentration of the solution alters the rectification coefficient. Quartz surfaces are characterized by hydron or hydroxyl groups groups depending on the solution pH[38]. By lowering the pH of the solution, the excess of negative surface charges are neutralized and this leads to a linear current-voltage response: at pH 3, which is in the range of the isoelectric point of quartz, the I-V curve shows a linear characteristic. The rectification becomes stronger at lower KCl solution concentrations and for concentrations above 0.1 M, the capillaries behave as an Ohmic resistor.[37] The electrical double layer is significantly reduced with an increase of electrolyte concentration, which leads to a lower impact on the ionic transport.[38]

The ICR can be modified by chemical functionalization of the inner walls and is very sensitive to the surface charge density and distribution.[21] The ICR magnitude can be described with a rectification coefficient (r), defined as the logarithmic ratio of the current value at the positive voltage to the current at opposite polarity with the same amplitude.

Yin *et al.*[39] reported that ICR is observed also in organic solutions with nanopipettes even if the rectification direction is opposite with respect to the ICR in aqueous solutions. In this scenario, the pore size, surface charge, electrolyte concentration and the water amount in the solution are crucial parameters.

Nonlinear I-V characteristics of quartz nanopipettes are affected by the relative dimensions of the electrical double-layer thickness and orifice and the rectification is only observed when the aperture dimension is comparable to the thickness of the electrical double layer. Further, ion transport properties at the tip are modified by solution pH and concentration.[38][37]

3.3 Geometry characterization of nanopipettes

Geometry and surface chemistry of quartz nanopipettes have a substantial impact on the response and an accurate geometry characterization becomes more crucial when the dimension of nanopipettes decrease. Transmission electron microscopy (TEM) and scanning electron microscopy (SEM) are commonly used to visualize the dimension of the nanopipettes.[23]

The key geometrical parameters to extract are the aperture size, the inner half-cone angle and the glass thickness. The size of the opening defines the resolution and the glass thickness at the tip can affect the nanopipette response.[40] In Fig.3.3 a schematic of a single pore nanopipette geometry is proposed.

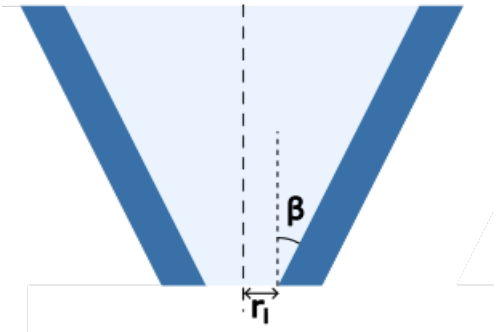

Figure 3.3: Schematic of the nanopipette tip, where r_i and β are the nanopipette radius and cone half-angle, respectively. Adapted work from [23].

From SEM images, an estimation of the aperture radius and the glass thickness at the opening is derived. The main drawbacks of the SEM are the low resolution that makes this method unsuitable for tip openings smaller than 50 nm and the required coating with a conductive metal film which modifies the nanopipette dimensions.[40] However, TEM measurements induce deformations on the pipette tip due to the heat caused by the electron-beam irradiation, but a more accurate estimation of the geometry parameter can be extracted.[23]

Perry *et al.*[40] propose the use of TEM to analyze the nanopipette geometry precisely and finite element method (FEM) simulations to match the obtained I-V results to extract the surface charge.

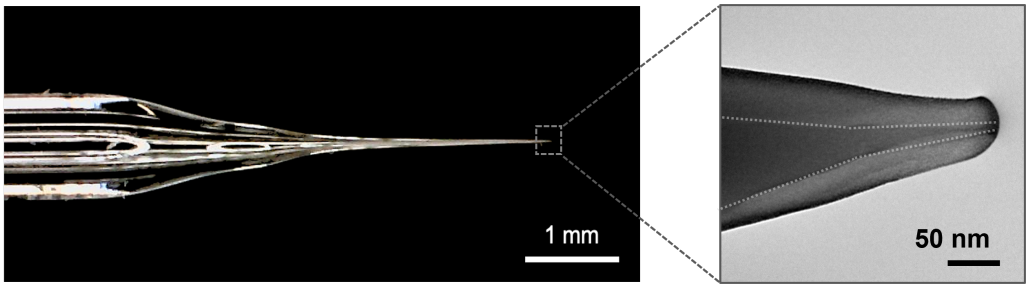

Figure 3.4: Optical microscope image of a nanopipette (left) with a magnified TEM image (right) that shows the opening size of ≈ 10 nm.[28]

Electrochemical methods can be used to estimate the inner nanopipette radius (r_i), and half-cone angle (β).

The first method assumes that the ratio between the inner and outer diameter of a nanopipette remains constant along the length, and the inner nanopipette angle can be extracted by applying the following equation[40]:

$$\tan \alpha_{inner} = \frac{\tan \alpha_{outer}}{r_{OI}} \tag{3.1}$$

where α_{outer} is the outer nanopipette angle, obtained from SEM analysis, and r_{OI} is the ratio between the outer and inner pipette radii at the tip. The assumption that the ratio is constant is underestimating the nanopipette resistive properties.[40]

Another technique is based on the nanopipette resistivity, estimated from I-V curves. The total resistance is composed of two components, i.e. the inner (R_{int}) and outer (R_{ext}) solution resistance; the resistance is dependent on the inner nanopipette radius and the inner half-cone angle according to[21][23]:

$$R = R_{int} + R_{ext} \approx \frac{1}{\kappa \pi r_i \tan \beta} + \frac{1}{4 \kappa r_i} \tag{3.2}$$

where κ is the solution conductivity. The inner nanopipette half-cone angle is estimated from image techniques, but it could vary along the length and due to pulling parameters. Even a small variation of the inner nanopipette angle could strongly affect the calculated resistance.[40][23]

The last method is based on the diffusion limiting current (i_d) equation[21][23]:

$$i_d = 4 x_i z F D r_i c \tag{3.3}$$

where D is the diffusion coefficient, F is the Faraday constant, z is the charge of transferred ions,c is the bulk concentration, and x is a paramter function of r_{OI}. From this equation, the tip radius can be estimated and then it can be used to evaluate the angle through Eq.3.2.

3.4 Filling nanopipettes

Filling a sub-10 nm pipette is a challenge due to the small aperture, but it is necessary to obtain a stable ionic current, and thus a reliable and precise measurement. Bubble formation at the tip is one main issue that prevents the current measurement since there is no conductive path. The adopted protocol requires filling the nanopipettes with a MicroFil syringe from the back of the nanopipette filament and this method is one of the fastest and easiest possible solutions, as also described by Simonis *et al.*[41]. With this back-filling technique the bubbles are not prevented, but bigger bubbles travel to the back and leave, while small bubbles stay at their positions and influence the ionic current while measuring. Injection speed of the liquid inside the nanopipette is a key factor in bubbles formation. By slowing the injection, bubbles can be reduced.[41]

Another proposed method for nanopipettes is based on electromigration. First, the nanopipette is filled with water and then the liquid is replaced with the desired electrolyte via electromigration.[42] This process can be applied to any nanopipette's shape and tip aperture, but this long and tedious techniques involves moving the water-filled pipette close to a heated filament which allows boiling the water and then the water re-condenses. The pipette is placed in a thermal loop until the deposited re-condensed water reaches micrometric dimensions; in this way, the droplets at the tip get smaller and smaller, and the tip can be filled with the proper electrolyte.[42] Few other procedures, but ineffective with the applied protocol, are proposed in literature: passive loading using a desiccator which requires longer time and more equipment, but it is be well suited in complex situations where it is hard to handle the nanopipette or when they show an unusual shape[41][42]; high pressure applied to the back of the nanopipette which could take days to fill and it does not apply to sub-10 nm since the tip would break due to the high applied pressure. Plasma treatment could enhance the surface wettability, but this step could lead to unwanted surface modifications.[42]

The most effective and fastest procedure to obtain a nanopipette without bubbles is presented by Sun *et al.* [43]. A temperature gradient is applied *via* to a hot plate and this technique allows the water vapour to move from the backside of the pipette to the tip region until all bubbles are removed. The proposed method uses a hot plate at 80 °C for 10 min. This last protocol has been used several times when bubbles were preventing to measure the ionic current, but a lower yet still effective, temperature of 55 °C was applied. The presence of a filament inside the nanopipette creates irregularities at the tip when melted and this eases the filling procedure.[42]

3.5 Double pore nanopipettes

Double pore nanopipettes are obtained from quartz capillaries with two pores separated through a quartz barrel (Fig.3.5a). Double pore nanopipettes could replace two single pore nanopipettes placed close to each other to perform multiplexed sensing in the same location. The main disadvantage of the two single pore nanopipettes system is the inability to position the two tips close enough (minimal distance on the tens of micrometer scale) to allow the two nanopipettes to detect the analytes in the same microenvironment. Given the density and complexity of brain tissues, even a micrometric distance between the two nanopipettes would lead to different environments and analyte concentrations. Functionalizing the two pores selectively with two different aptamers would lead to the development of multiplexed biosensors with the possibility to have a sensor pore and a control pore or two sensor pores to detect two different analytes.

Common applications of double pore nanopipettes are DNA and single-molecule manipulation[44], protein detection through extended field-effect transistor[45], high-resolution 3D printing[46] and DNA counting[44].

A three-line pulling program and the alignment of the quartz barrel to the ground during the pulling should lead to two pores with similar apertures. Pore similarity is analyzed by comparing the magnitudes of the real-time current response of the two pores and by performing cyclic voltammetry to extract the rectification coefficients and the working current range. Having two pores with comparable dimensions is crucial to compare the two current responses upon analyte detection.

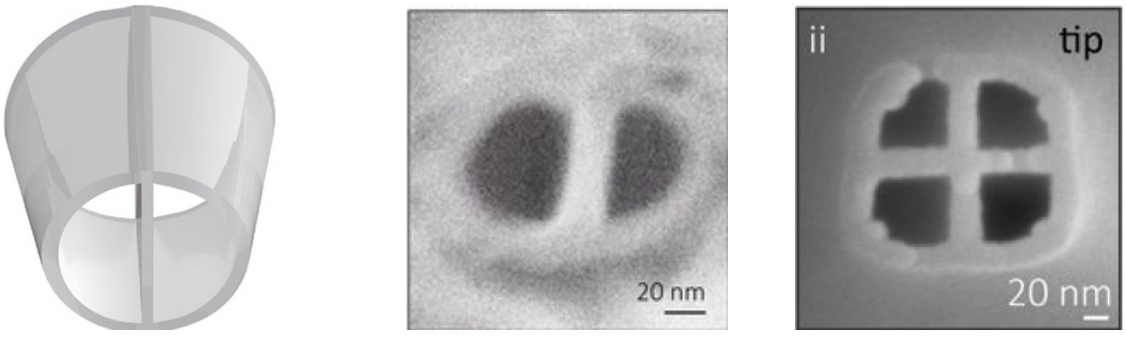

(a) **(b)** **(c)**

Figure 3.5: (a) Schematic of the tip of a double pore nanopipette.[45] (b) Transmission electron microscopy image of double pore nanopipettes' tip.[44] (c) Bright-field and scanning electron microscpy images of the quad-barrel nanopipettes' tip aperture.[47]

SEM (Fig.3.6) and TEM (Fig.3.5b) provide a detailed look at the tip to characterize the tip geometry and estimate the two pore dimensions aside the current response comparison. The two imaging techniques show the same advantages and disadvantages as for single pore quartz nanopipettes.

A further improvement in the multiplexed biosensing direction would be functionalizing a quad-pore nanopipette with two sensor pores and two control pores as illustrated in Fig.3.5c.

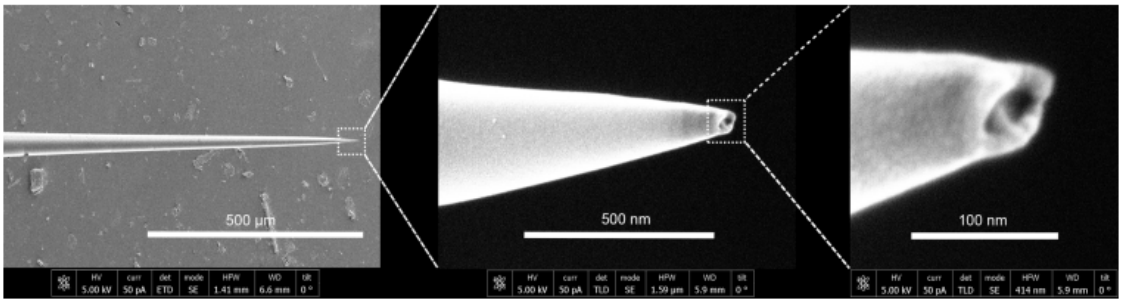

Figure 3.6: Visualization of double pore nanopipette using SEM.[32]

Chapter 4

Results

4.1 Silane chemistry: double pore functionalization

Obtaining dopamine-sensitive sensors requires the functionalization of the bare quartz surface of nanopipettes. Aminosilanes are assembled on the surface that are, then, coupled to the thiolated aptamers. In Fig.4.1a the functionalization protocol is illustrated. These steps have been validated and used for serotonin[31] and dopamine aptamer-modified single pore nanopipettes.

In double pore nanopipettes, functionalizing selectively one pore, while leaving the other one empty, is not trivial (Fig.4.1b). The standard functionalization protocol for single pore nanopipettes cannot be completely transferred because the aminosilanes groups make the surface hydrophilic. This hydrophilicity of the surface is responsible for the liquid crawling from the pore to functionalize to the empty one creating a liquid bridge at the tip. Cross-contamination leads to both pores being functionalized at the tip and reactive to dopamine, as depicted in Fig.4.3d. Being able to selectively functionalize one pore is the first step toward the functionalization of the two pores with two different aptamers, *e.g.* the dopamine aptamer and the control sequence or two specific aptamers such as dopamine and serotonin.

The first promising method to functionalize properly one pore is the voltage applied method.[32] This technique is commonly used in DNA translocation experiments[44][48] to drive DNA strands or aptamers. Applying a potential influences electrically the location of aptamers due to the negative charge. A positive voltage attracts the negative aptamers, while a negative voltage rejects them. The functionalization protocol remains unchanged until the aptamer incubation is substituted with the voltage applied technique. In Fig.4.2a the basic principle is described: a voltage difference is applied between the two pores filled with PBS, where the positive voltage is applied in the sensor pore and the negative voltage to the empty pore, and, then, the nanopipette is lowered in an aptamer solution. The positive voltage applied to the sensor pore attracts the aptamers to move from the bath to inside

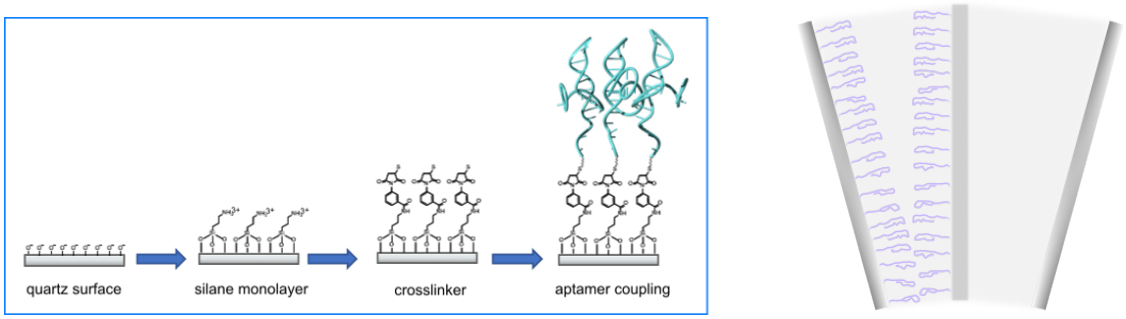

(a) **(b)**

Figure 4.1: Dopamine aptamer functionalization on quartz nanopipettes. (a) Schematic of the functionalization protocol. A layer of aminosilanes (NH_3^+ groups) is assembled via vapour-phase deposition on quartz nanopipette walls where thiolated dopamine aptamers couple covalently on the surface. (b) Illustration of the functionalization goal: being able to selectively functionalize one pore, while leaving the other one empty: Sensor (left) pore *vs.* Control (right) pore.

the sensor nanopore that should bind to the already present chemistry. Meanwhile, the negative voltage applied to the empty pore should prevent aptamers to enter inside the nanopore; this should block any functionalization in the empty nanopore. Before lowering the nanopipette in the aptamer bath the voltage difference between the two pores should be applied to avoid aptamers to bind on the surface of the empty pore. Several voltage differences have been applied, from 1.2 V to 4 V, but, at any applied voltage, the two pores showed the same behaviour and rectification. A functionalized nanopipette shows a higher rectification than a bare one since the rectification is charge-dependent aside pore size dependent; the expected result is shown in Fig.4.3a where the two pores exhibit two different rectifications. In Fig.4.3c the typical result is depicted: the two pores show the same rectification, and the hypothesized obtained functionalization is illustrated in Fig.4.3d. The hypothesis that the aptamers are not completely blocked from entering the empty pore, with both pores being functionalized, is still valid for this functionalization protocol.

A variation to this first described voltage applied technique has been tested as well (Fig.4.2b). In this configuration, two independent negative biases are applied to the empty pore and the bath, while the sensor pore is filled with the aptamer solution. The negative voltage applied to the bath (V_{BATH}) should prevent the aptamers to leave the pore to be functionalized. A negative bias, higher in magnitude than V_{BATH}, is applied to the empty pore to block aptamers to accede. The voltages are applied before filling the sensor pore with the aptamer solution to avoid further possibilities of cross-contamination. This second voltage applied technique has been tested a few times without any valuable results.

These two voltage applied methods are time-consuming, ~ 5 h to functionalize four nanopipettes without obtaining any working double pore nanopipette. Neither of the

two pores of the tested nanopipettes was reacting to dopamine, so the hypothesis was that functionalization was not happening at all in the two pores. To validate this idea, several DNA translocation experiments with single pore nanopipettes were carried out with the dopamine aptamers to acquire new insights into the functionalization process (see 4.2 section).

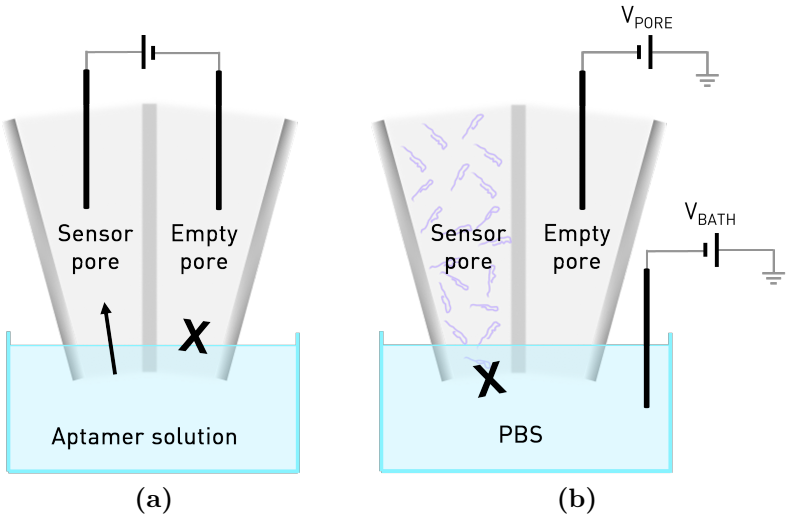

Figure 4.2: Configurations of the voltage-applied protocol. (a) A voltage difference is applied between the two pores with the positive voltage applied to the sensor pore to attract the negatively charged aptamers from the bath to the nanopipette. (b) Two different negative voltages are applied to the empty pore and the bath. The aptamer solution is inside the sensor pore and the negative voltages should prevent the aptamers to escape from the sensor pore.

In Fig.4.4 a summary mind-map of all the variations applied to the standard functionalization protocol is presented. The capillaries are typically pulled before undergoing the functionalization protocol. Since the liquid crawling is happening at the tip, pulling the capillaries at the end of the functionalization could prevent cross-contamination. One pore of the capillary is functionalized while it is still a quartz cylinder. With this proposed method, the double pore capillaries are following the same functionalization protocol used for single pore nanopipettes for the sensor pore. Functionalizing the centre area of the capillary, where the tips of the nanopipettes will be formed, and being able to maintain the capillary flat during the functionalization protocol to avoid liquid crawling at the ends are crucial key factors. One issue is the pulling since only dry capillaries should be inserted in the puller to create the nanopipettes. Solution droplets spread during the pulling affect the quality of the mirrors in the puller which compromises the tip of the nanopipettes. Moreover, aptamers could suffer from the high applied temperature during the pulling. Few nanopipettes have been tested after pulling being wet and the two pores showed the same behaviour in terms of rectification, instability in current during real-time

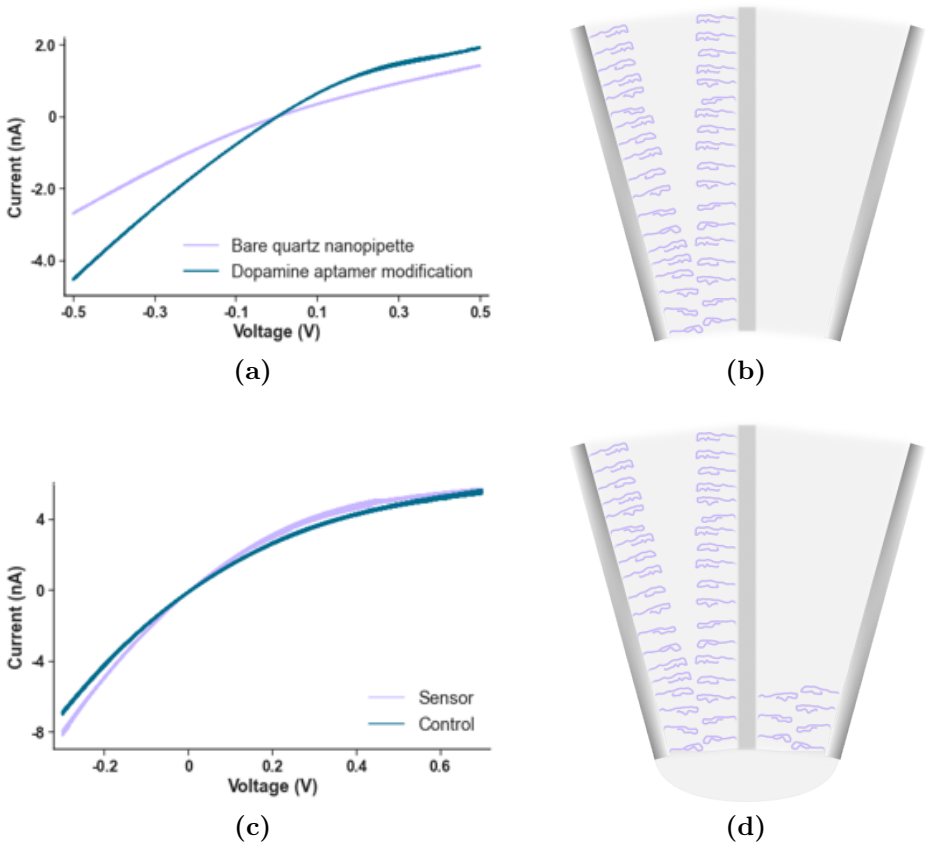

Figure 4.3: (a) Cyclic voltammetry of the sensor and empty pore after functionalization. (b) Cross-contamination hypothesis to explain the similar rectification after the functionalization protocol.

measurements and large current values ($\sim$ 7 to 9 nA at 0.5 V).

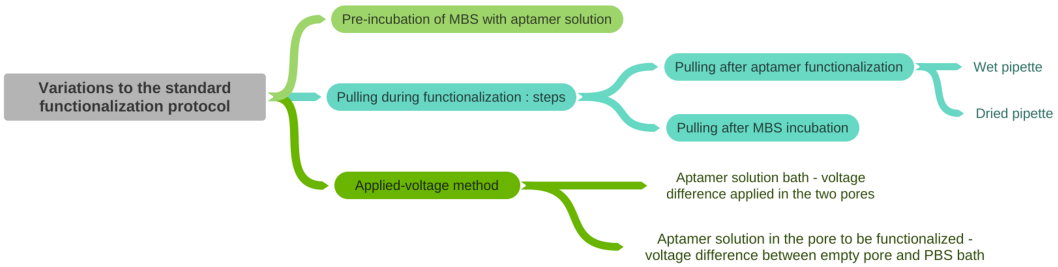

Figure 4.4: Schematic of the various functionalization protocols for double pore nanopipettes.

To avoid this pulling issue with wet capillaries, various drying techniques have been analyzed: simple overnight air drying, oven at 50 °C for 30 min, N_2 flow and

the desiccator. Any of these techniques seem to be promising and feasible with the actual functionalization protocol. The heat from the pulling is probably too high and damages the bonds of the different layers.

4.2 DNA translocation through nanopipettes

The functionalization of double-barrel capillaries is not trivial and several approaches have been investigated with the goal of functionalizing only one pore with the desired aptamer while leaving the other pore empty. The main issue that arises from the standard functionalization protocol is cross-contamination at the tip. The liquid is crawling from one pore to the other one due to the highly hydrophilic surfaces after aminosilane functionalization. This cross-contamination results in both pores being functionalized with the same aptamer and thus reactive to the same analyte. A promising functionalization protocol of double-barrel pipettes consisted of a method that electrically influenced the location of aptamers by applying voltage biases. [32] Due to the negatively charged phosphodiester backbone, aptamers are attracted to the pore where a positive voltage is applied, while aptamers are rejected by a negative voltage. The pipette tip is immersed in an aptamer solution, and a positive voltage is applied to the pore to be functionalized and a negative voltage to the pore where aptamers should be prevented from entering. The tested pipettes from several batches were not reacting to dopamine and both pores showed the same rectification; the main hypothesis was the inability to take up aptamers from the solution through the nanoscale aperture. To test this hypothesis, single pore pipettes have been employed in several DNA translocation experiments to analyze the feasibility of this voltage-applied protocol. The translocation of the aptamer through the pore, from the bath to the pipette and vice-versa, could be visualized as peaks in the current response.

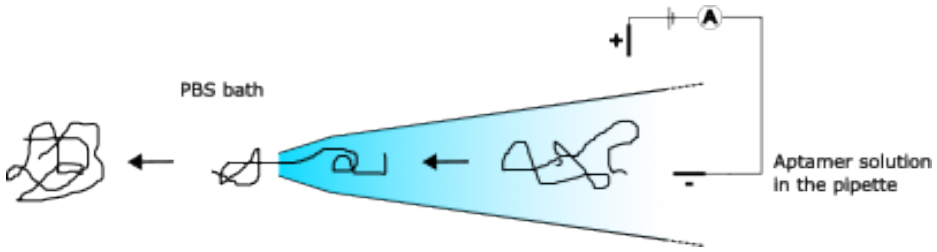

Figure 4.5: Set-up configuration for the conducted experiment of DNA translocation.

Two different configurations have been tested: a pipette filled with PBS is lowered in an aptamer bath. When a negative voltage is applied to the bath (positive bias in the nanopipette), the aptamers should transverse from the bath to inside the nanopipette. In the second investigated system the pipette is filled with the aptamer solution and inserted into a PBS bath. Then, positive voltage is applied to the bath and, through electrostatic interactions, aptamers are attracted to move from inside the pipette to the bath. In both scenarios, a peak in the current response is expected when the event is taking place, but in different directions: a drop in current when the DNA strand moves from the bath to the pipette and an increase in current for the alternative path.[49] The set-up of the second described experiment, as well as

the DNA translocation event from inside the pipette to the external PBS bath, is depicted in Fig.4.5. In the studies conducted by Bell *et al.*[49] and Fraccari *et al.*[50], the expected translocation time should be in the sub-microsecond range given the short length of the dopamine aptamer (44 nucleotides). Thus, the sampling frequency of the amplifier was adjusted to $f_s = 500\,\text{kHz}$, so the sampling time $T_s = 2\,\mu\text{s}$, without any point average to visualize the peak in the current response.

The first configuration is an experimental simulation of the standard functionalization protocol where voltage biases are applied. The goal was to test if aptamers could transverse from the bath to inside the pipette. A pipette filled with PBS is lowered into an aptamer bath after being functionalized with aminosilanes to create a positively charged surface that would attract negatively charged DNA. This experiment was repeated four times (N=4, with four different pipettes), but no peaks were observed in the current response. A positive bias is applied inside the pipette and, at each voltage step, the current was stable without variations in the baseline. In literature, 10 nm quartz nanopipettes have been successfully used in long-chain DNA translocation experiments with double-strand DNA[51] and nucleotides[52]. Bell *et al.*[49] investigated the translocation time of aptamers from the bath to inside the pipette and vice-versa and from the model they extracted the translocation time of a double-strand DNA with 3 000 basepairs is lower than 100 µs.

Taking this report into consideration, the short dopamine aptamer (44 nucleotides) may not be observed due to the limitation of the amplifier resolution since the shortest time between two data points is 2 µs. In the literature, several methods to reduce the translocation time have been presented.[53] However, no experiments have been conducted in this direction to confirm the amplifier-limited hypothesis.

The set-up is then reversed for the second experiment configuration: a pipette filled with an aptamer solution with the same previous concentration is lowered in a PBS bath where a positive voltage is applied. The typical peaks in the current response could be visualized under these conditions.

The peak direction appears to be dependent on the surface charge of the pipette, which is a key finding from this experiment (Fig.4.6). When an aptamer translocation event occurs, upwards peaks from the baseline can be noticed for bare unfunctionalized pipettes that have a negatively charged surface. Downward peaks were observed for pipettes that had been previously aminosilanized and thus had a positively charged surface. The hypothesis is that when the negatively charged DNA aptamer passes through the small aperture with charged walls, there is a different charge interaction.

The two peak directions can be observed in Fig.4.6 and the experiment was repeated N=5 times with three aminosilanized pipettes and N=3 with three bare pipettes. The peak direction of bare pipettes is consistent with examples in the literature.[49][44] This surface charge dependence was not found for larger pores. Bare pipettes with a pore opening of 30–50 nm show both peak directions within the same

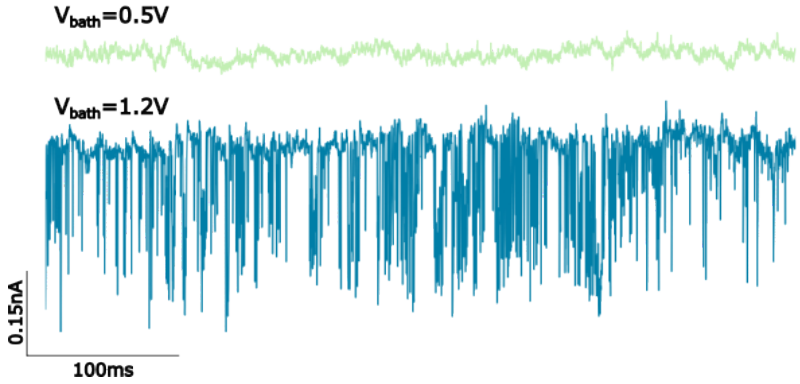

(a) Aminosilanized nanopipette with positive surface charge.

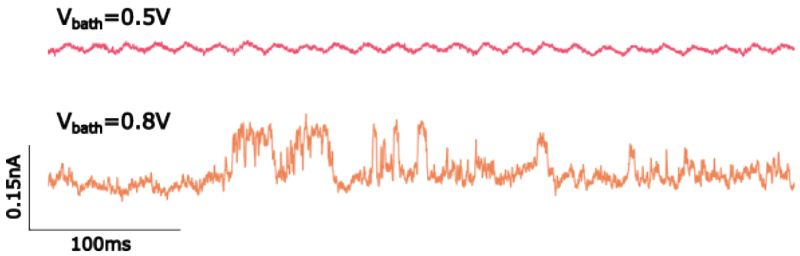

(b) Bare unfunctionalized pipette with negative surface charge.

Figure 4.6: Peak direction dependent on nanopipette surface charge at different voltages.

pipette. This behavior has been observed for N=2 with two pipettes with 30–50 nm pores. The peak direction seems to be strictly related to the surface charge of the nanopipette, but also to the aperture's size since both peak directions were found in bigger pore pipettes. This behavior could be related to the diverse interactions that the aptamer could have with the charged surface. The aptamers and the surface are charged element and, thus, electrostatic forces arise. Attractive and repulsive forces are involved in the interaction depending on the sign of the charged species. A quartz nanopipette in an electrolyte solution forms an ionic electrical double layer on the surface.[38] The thickness of this electrical double layer is defined as the Debye Length, which scales with ionic concentration and is < 1 nm for the undiluted physiological buffer solution used in the experiments.[28] The greater the relative area composed of the double layer with respect to the aperture area, the stronger the influence on the ionic flux through the nanopipette. Thus, in the ~ 50 nm pore nanopipettes, the electrical double layer impacts the ionic flux less than in the 10 nm pore nanopipettes. Furthermore, in the ~ 50 nm pore nanopipettes, depending on the position where the aptamer translocation is happening, the interaction between the

aptamer and the charged surface can vary since only in small area is occupied by the electrical double layer, which affects the electrostatic interactions. Such variations in electrostatic interactions between the negatively charged aptamers and the quartz surface (bare *vs.* aminosilanized) may lead to divergent peak directions.

The peak amplitude appears to be related to the applied voltage, so the peak amplitude should increase when a higher voltage is applied.[44][48] However, during the conducted experiments with 10 nm aperture pipettes, it was not possible to notice any peaks before a voltage threshold and, the amplitudes of the peaks showed a similar magnitude at different voltages.

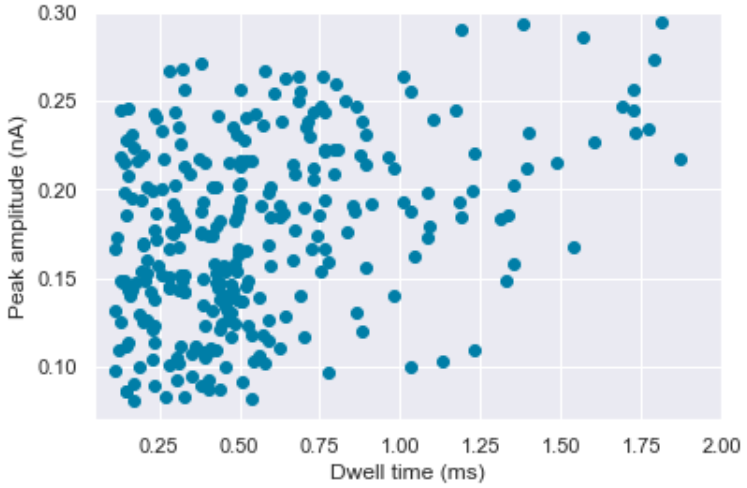

Figure 4.7: Dwell time and peak amplitude analysis of the silanized pipette shown in 4.6 for the same time slot.

In Fig.4.7 a peak analysis is reported on the same span of the aminosilanized pipettes in Fig.4.6 with a closer look at peak geometry: amplitude and width. The width has been measured at 15% of the peak height to avoid adding any noise peaks to the statistics. A period span of 500 ms and N=313 peaks with a magnitude greater than 80 pA were recorded. This arbitrary threshold is based on the noise level of the baseline. As expected from the literature, the mean width is in the sub-microsecond range.[49][50] The higher width values could be related to multiple DNA translocations or to the different shapes that the peak can show related to the several folding shapes that the aptamer can assume at the pore.

In Fig.4.8 there are four different peak shapes that were recorded for aminosilanized pipettes. Peak's shapes are related to several factors: aperture size and geometry, folding mode of the aptamer,[54][49] and applied voltage[50]. Aptamers can assume a variety of geometrical and folded configurations, resulting in a different event peak in the current response. A higher voltage results in a peak with a larger amplitude and with a peak-like shape, whereas a lower voltage results in less steep

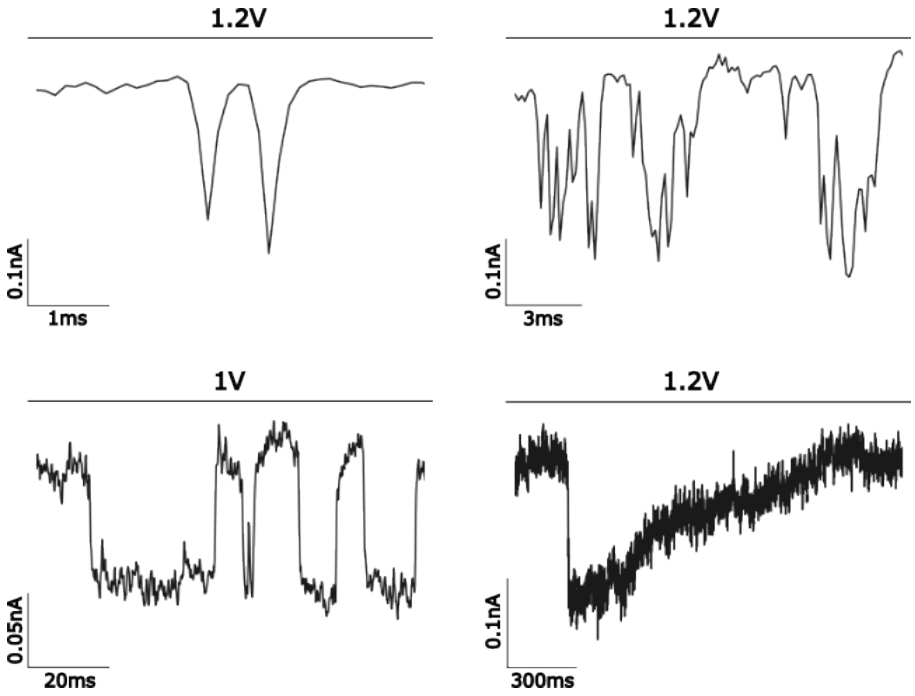

Figure 4.8: Peak shapes obtained during the DNA translocation experiments with aminosilanized pipette.

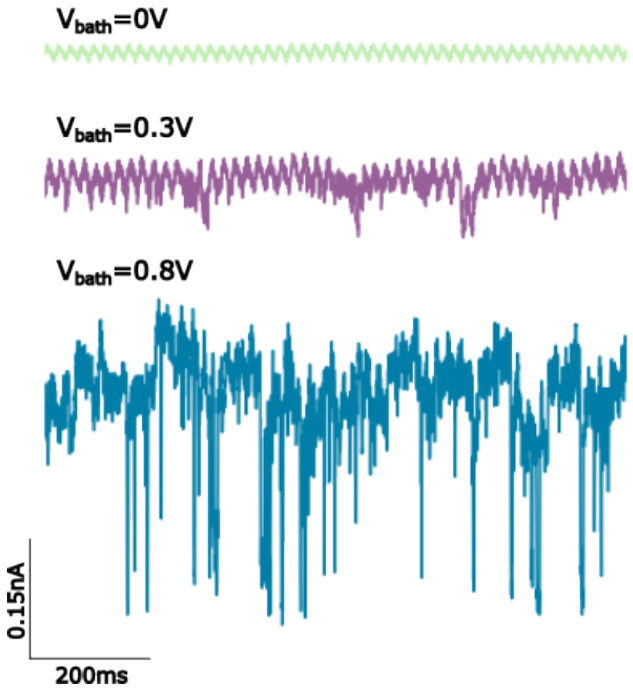

Figure 4.9: Peak amplitude dependence on the applied voltage.

peaks and peaks with a more rectangular shape.[50] The amplitude is related to the pore geometry. The amplitude of DNA translocation events with a larger pore of 30–50 nm can be analyzed in Fig.4.9: the amplitude is increasing with a higher applied voltage.

Throughout these experiments the results presented in literature have been successfully replicated while identifying the influence of surface charge on peak directions.

4.3 Alternative functionalization protocol

After several failures to functionalize double-barrel nanopipettes following the silane functionalization protocol, a new possible functionalization emerged to link the quartz surface of nanopipettes with aptamers. The stack is composed of a monolayer of biotinylated poly(L-lysine)-graft-poly(ethylene glycol) (PLL(20)-g[3.5]- PEG(2)/PEG(3.4)-biotin(15%)) which is bridged to the biotinylated aptamers through streptavidin molecules as depicted in Fig.4.11.

PLL-g-PEG is a random graft co-polymer with a poly(L-lysine) backbone and poly(ethylene glycol) side chains. This polymer is a self-sorting double network hydrogel where the PLL backbone interacts electrostatically with the quartz surface while the PEG chains form a densely packed polymeric brush. This polymer is self-limited to forming a monolayer coating, giving reproducible and constant thickness.[55] Graft polymers are co-polymers with a linear backbone (PLL) and randomly distributed branches of another composite (PEG). There is a covalent bond between the two composites.[56] The main properties of PLL are: positively charged for pH$<$ 10, high coverage on the surface and kinetic inertness. PEG is a hydrophilic and uncharged polymer with flexible chains.[55] In Fig.4.10, the comparison between the real PLL-g-PEG with biotinylated PEG chains and the illustration is shown.

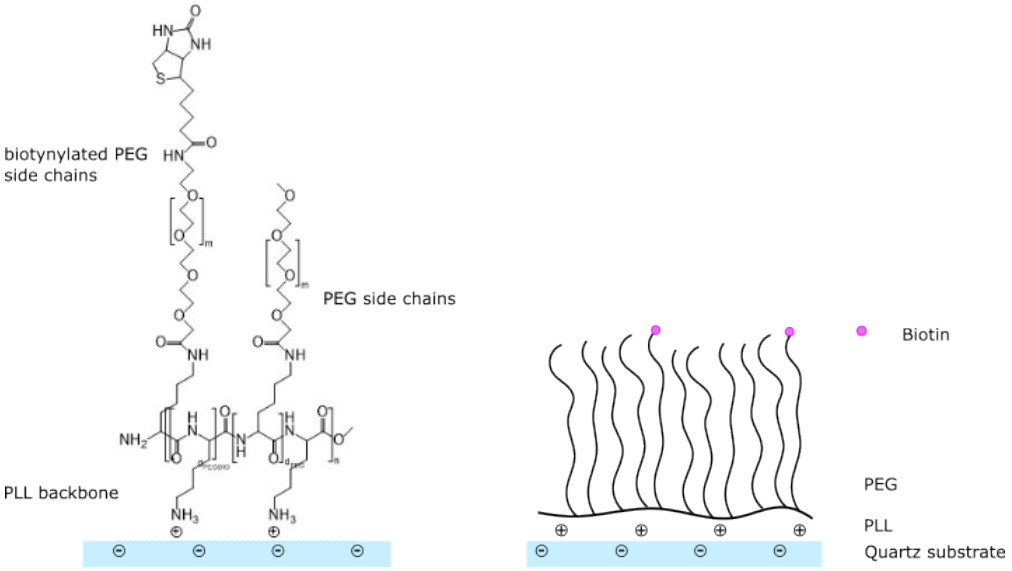

Figure 4.10: PLL-g-PEG real molecule schematics in comparison to the functionalization illustration.

PEG chains are functionalized with biotin to take advantage of the strong bond between biotin and avidin to bind the aptamers on the surface. The biotin-avidin bond is one of the strongest non-covalent bonds in nature and characterized by high affinity, high specificity, high stability, and low perturbation.[57] Streptavidin is a tetravalent biotin-binding protein which shows less non-specific binding with

respect to avidin.[58] Each subunit shows the same affinity to biotin. This high affinity between avidin and biotin is given by an extensive network of hydrogen bonds, as well as Van der Waals force-mediated contacts and hydrophobic interactions.[57][59]

As illustrated in Fig.4.11, the functionalization protocol to modify bare quartz nanopipettes into dopamine sensors consists of two incubations: firstly PLL(20)-g[3.5]-PEG(2)/PEG(3.4)-biotin(15%), and, then, the steptavidin-biotinylated aptamer complex. The biotinylated aptamers are pre-incubated with streptavidin to occupy, on average, two of the binding spots before the incubation inside the nanopipette to allow the binding to biotin present on the PLL-g-PEG coating. This functionalization protocol is faster, easier and less subjected to environmental variations (such as temperature and humidity) than the standard functionalization protocol. This technique takes maximum 1.5 h to obtain the complete stack, while the silane chemistry requires $\sim$ 5 h. The main overcome issue is the aminosilanization step which is not fully controllable and highly humidity dependent. One characteristic of the layer-by-layer functionalization is its thickness that is $\sim$ 15 nm (Fig.4.11) while the tip orifice is $\sim$ 10 nm. In Fig.4.12 the illustration in scale of possible spatial organization of the layer-by-layer functionalization at the tip.

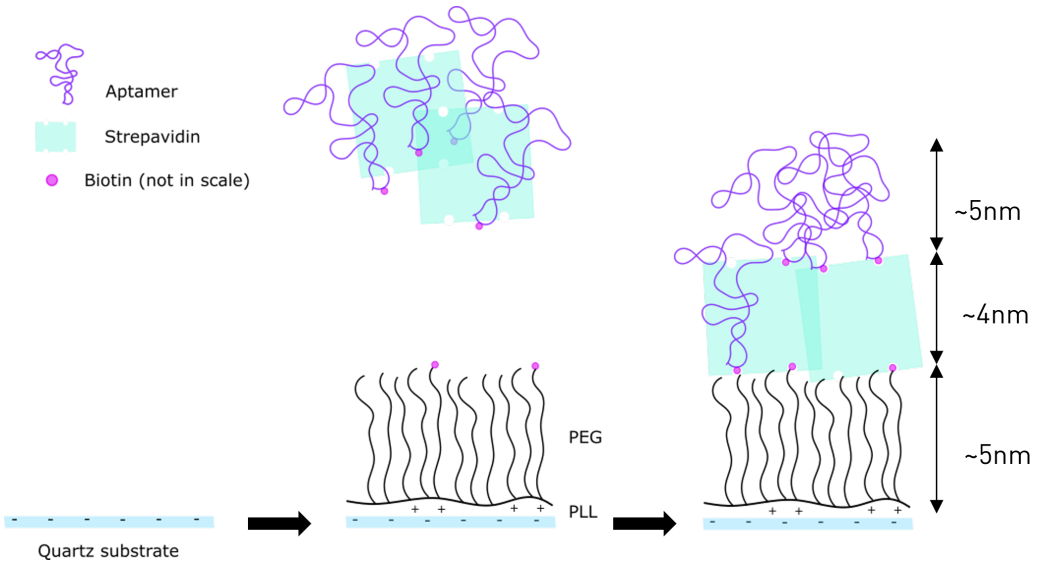

Figure 4.11: Illustration of functionalization protocol the tip showing a possible conformation of the stack. The PLL-g-PEG, Streptavidin and aptamer thickness are in scale to the tip thanks to the obtained data from QCM-D experiments in accordance with the literature.

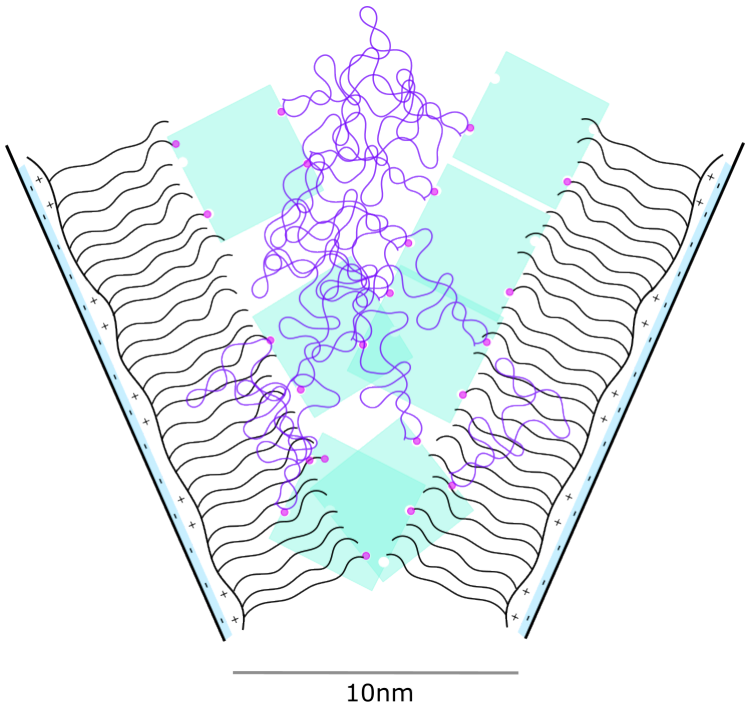

Figure 4.12: Illustration of the tip showing a possible conformation of the stack. The PLL-g-PEG, Streptavidin and aptamer thickness are in scale.

4.3.1 Results and discussion

The layer-by-layer functionalization was investigated through the change in ICR characteristics in PBS by comparing the rectification at the different functionalization steps (Fig.4.13a). Due to the negatively charged aptamers, the aptamer assembly alters the ICR to a negative rectified surface. The negative rectification is tuned by the pore size and the aptamer density on the surface.[31] The bare quartz nanopipettes show a slightly negative rectification due to the negative charges present on the quartz surface (purple curve in Fig.4.13a). After the PLL-g-PEG incubation (blue curve in Fig.4.13a), nanopipettes should exhibit a positive rectification due to the positively charged PLL backbone and uncharged PEG chain and biotin.[55][58] However, nanopipettes reveal an increased negative rectification after PLL-g-PEG incubation. The streptavidin-aptamer complex binding to the present PLL-g-PEG (light blue curve in Fig.4.13a) increases the negative rectification with the negatively charged aptamers[31] and uncharged streptavidin protein at physiological pH[60].

The pore size has a considerable impact on the ICR. In Fig.4.13b $N = 9$ current-voltage curves of functionalized working nanopipettes are displayed. The considered operation current range is between $\sim 0.7\,\mathrm{nA}$ and $4\,\mathrm{nA}$ at $0.5\,\mathrm{V}$ in PBS and the current variability is quite broad in this range. After the functionalization, the current-voltage measurement and the rectification coefficient in the buffer solution are possible verifications of the actual aptamer functionalization.

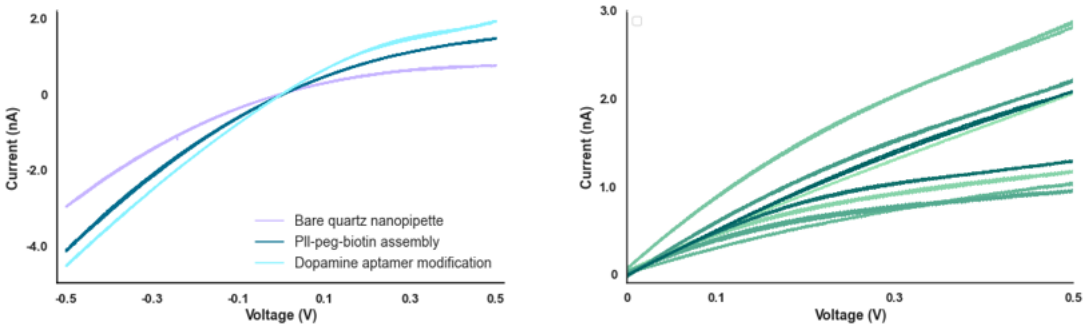

(a) **(b)**

Figure 4.13: (a) Current rectification at different steps of the functionalization protocol. (b) Current variability and various rectification for dopamine aptamer functionalized nanopipettes.

Various experiments have been conducted to interrogate dopamine aptamer-modified nanopipettes' specificity and selectivity. The first analyzed characteristic is the effective dopamine reaction and sequence specificity in PBS (Fig.4.14a). Current variation between the baseline current in PBS and the dopamine solution with a saturated concentration (100 µM) was recorded for dopamine aptamers and control sequence nanopipettes. The control sequence is a scrambled dopamine aptamer: the same number of base pairs of the dopamine aptamer placed in a random order which is not selective and specific for dopamine molecules. The current variation was normalized to the initial current in the buffer solution. Measurements with the control sequence give negligible dopamine responses. The dopamine response in PBS is expected to be in the range $0.1 - 0.35$ nA: this range is broad but correlated to the baseline current as a higher current variation is expected from nanopipettes with a higher baseline current value. The dopamine response is experienced as a decrease in current to the initial baseline current; the same direction of reaction occurs to dopamine aptamer-modified nanopipettes functionalized with the silane chemistry. The same experiment was conducted in artificial cerebrospinal fluid (aCSF), which exhibits a different ionic content that mimics the fluid in real applications. A similar result is obtained in PBS and aCSF as buffer solutions.

The specificity of the dopamine aptamer-modified nanopipettes is analyzed through current-voltage curves aside from real-time current variation. In Fig.4.15, current-voltage measurements with dopamine aptamer and control sequence nanopipettes reveal the current variation upon dopamine addition for the dopamine-specific aptamer in PBS. The control sequence measurement remains unaffected. The current values have been normalized to the initial buffer baseline.

The selectivity of dopamine aptamer-modified nanopipettes towards similarly structured neurochemicals in PBS is interrogated: the nanopipettes were exposed sequentially to PBS, norepinephrine, a neurotransmitter precursor of dopamine,

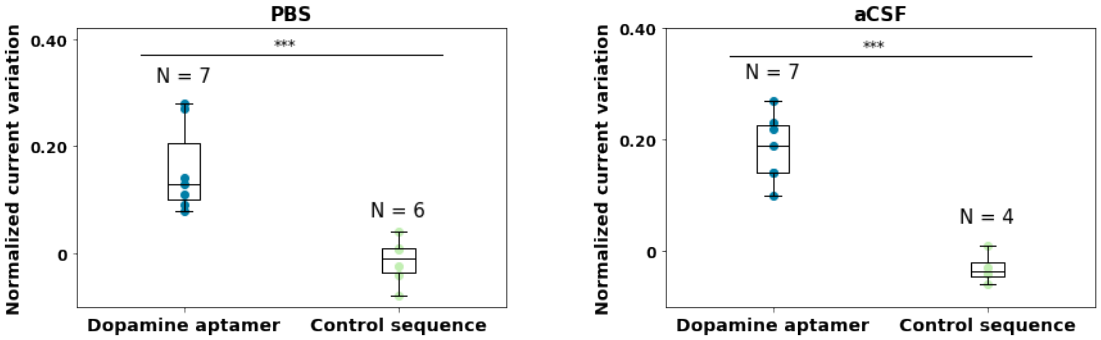

(a) (b)

Figure 4.14: Normalized current variation in (a) PSB (b) aCSF.

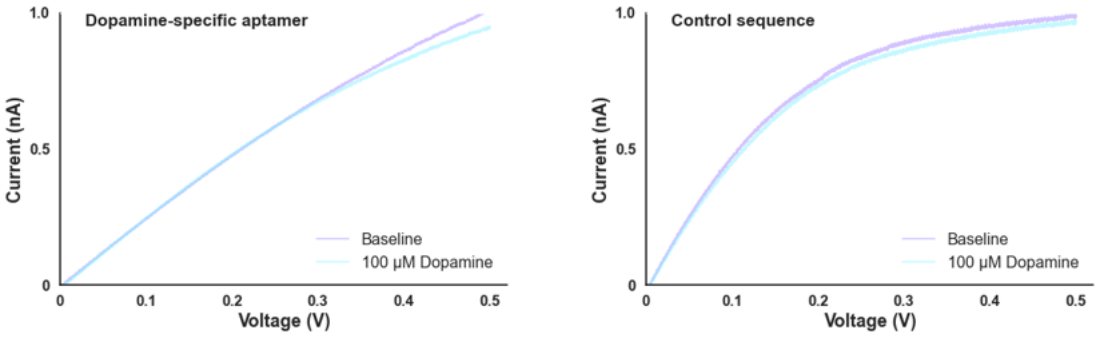

(a) (b)

Figure 4.15: Normalized cyclic voltammetry measurements in PBS of (a) dopamine aptamer modified nanopipettes and (b) control sequence upon dopamine 100 µM injection.

levodopa, another dopamine precursor, and dopamine at saturated concentrations (100 µM). In Fig.4.16a an example of real-time measurement. The first current instability during PBS injection in flow is due to the first liquid injection, which can vary slightly from the baseline current. Despite comparable molecular structures, after norepinephrine and levodopa injections, the current shows a negligible variation to the initial PBS baseline current, while a significantly greater response is observed when dopamine solution is pumped. The dopamine aptamer-modified nanopipettes selectivity was tested with $N = 3$ sensors with similar responses (Fig.4.16b): the response upon dopamine injection is in the expected working range, while an insignificant response is recorded after levodopa and norepinephrine.

Proven this polymer-based functionalization technique is specific and selective, the new characteristic to verify is the reset-ability of nanopipettes after dopamine detection. Reset-ability is the capacity to return to the current baseline value after

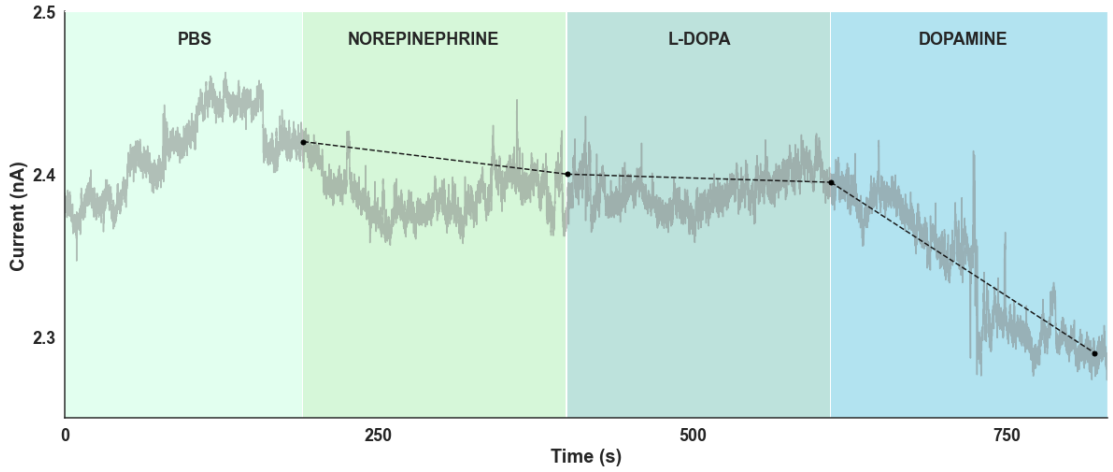

(a)

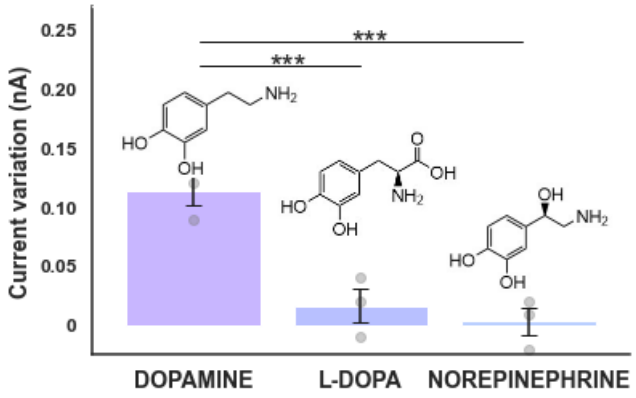

(b)

Figure 4.16: Selectivity analysis of dopamine aptamer-modified nanopipettes in flow to similarly structured molecules. The sensors were tested with Norepinephrine, Levodopa and Dopamine at 100 µM in phosphate-buffered saline. (a) Real-time measurement of the sensor while exposed to the three different analytes. This experiment has been successfully repeated with three different nanopipettes. The coloured regions are related to the injection time and the time needed to reach current stability before the next injection. (b) Boxplot shows the sensors' selectivity reproducibility with ***P<0.001. Error bars refer to the standard error of the mean for N=3.

dopamine detection. This characteristic is necessary to perform multiple dopamine detection over time in real applications. Current-time measurements with manual baths exchange (Fig.4.17a) and in flow set-up (Fig.4.17b) show the potential of nanopipettes to reset. The current after dopamine release, during the reset current, is not always the same as the initial PBS baseline, but a variation in the initial baseline direction is noticed.

Current-voltage measurements are another tool to investigate this reset-ability feature (Fig.4.17c). The current is reduced upon dopamine detection (dark blue), and then in the reset PBS bath (light blue) the curve is almost overlapping the initial PBS curve (purple). This ability to go back to the baseline current is not shown in all the nanopipettes that react to dopamine. Another scenario is given by the aptamer-modified nanopipettes that remain at the same current upon dopamine binding without being able to release dopamine molecules. Nanopipettes can typically reset to the initial current when placed in the initial buffer solution. Performing a few tens of cyclic voltammetry sweeps eases the reset behaviour.

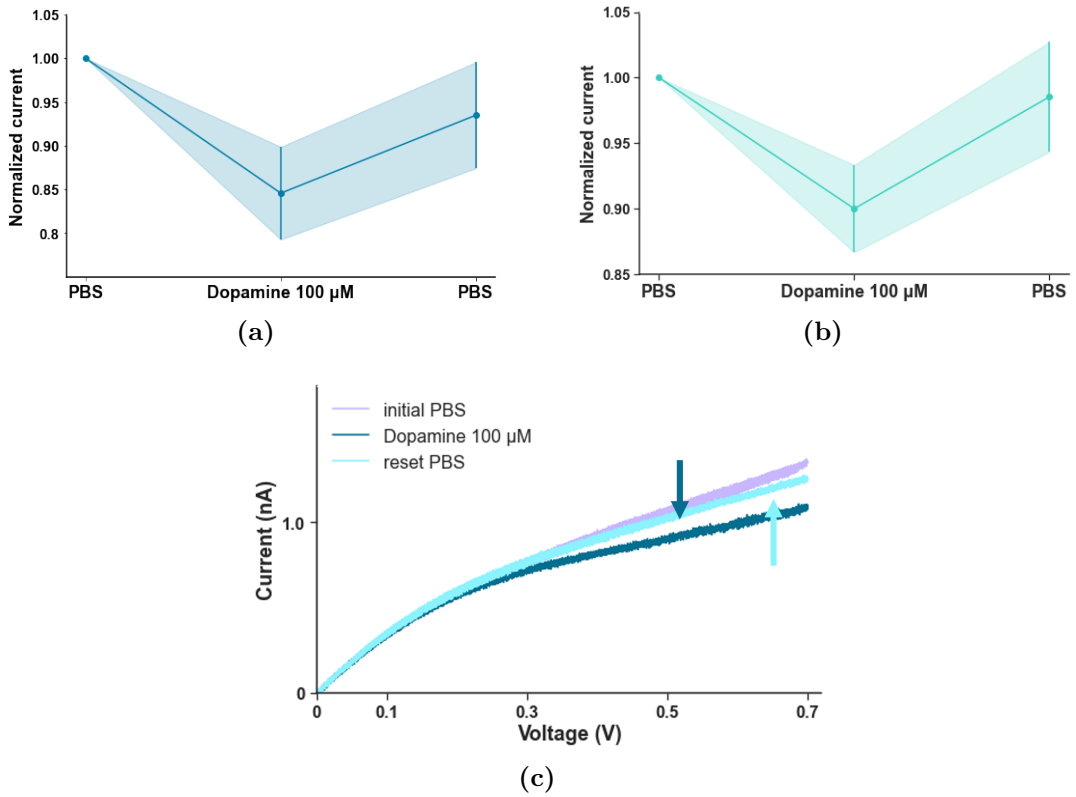

Figure 4.17: Reset-ability of dopamine aptamer-modified nanopipettes (a) by using different baths solution (N=3) (b) in flow with real-time measurements (N=5). A solution of 100 µM in phosphate-buffered saline was used. The current was normalized to the initial current baseline. (c) Dopamine reaction and reset-ability through cyclic voltammetry measurement.

In Fig.4.18a, another example of real-time measurement in flow is proposed to stress the importance of having aptamer-modified nanopipettes that can reset. After the dopamine injection, the current is subjected to a $\sim$ 15 nA decrease, and then after the PBS injections, the current is at a comparable value to the first PBS injection. Pumping PBS multiple times is needed to remove the dopamine solution since the

sensors are sensitive in the picomolar range. An highlight of different current levels taken at the pink dots is suggested in Fig.4.18b. Before pumping the new solution, the current was stable at least for 25 s. The current variations from PBS to dopamine solution and from dopamine solution to the final PBS are comparable.

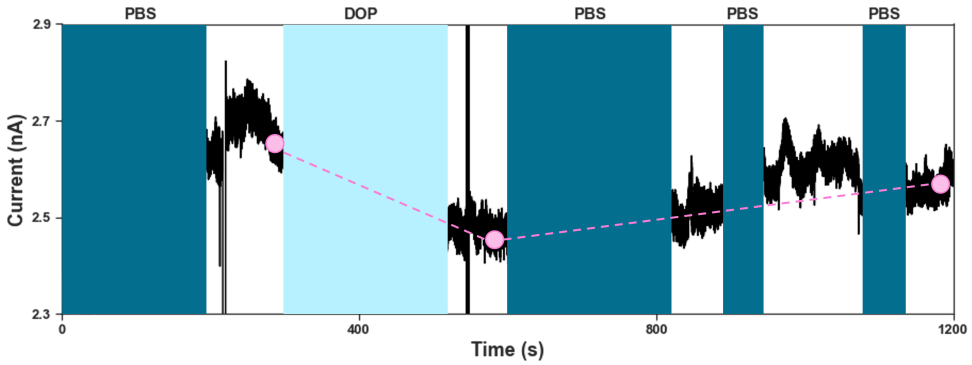

(a)

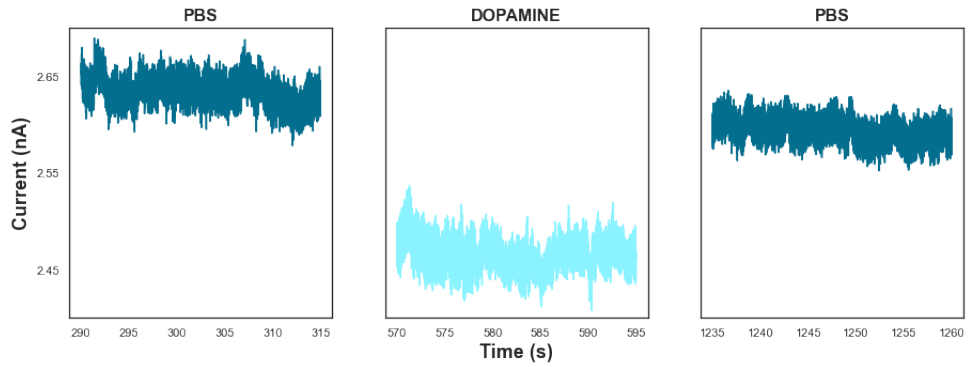

(b)

Figure 4.18: Real-time measurements to highlight the reset-ability of dopamine aptamer-modified nanopipettes. (a) Real-time recording with the different coloured regions related to the solution injection periods. PBS and dopamine 100 µM (DOP) are pumped in the mold. (b) Extraction from the real-time measurements to show the reaction magnitude and reset-ability. Time periods of 25 s for each bath.

The step closer to real applications is testing aptamer-modified nanopipettes in flow upon multiple dopamine injections (Fig.4.19a). Real applications reveal the necessity to detect dopamine multiple times over larger periods. With different sensors ($N = 3$) dopamine was detected 3 times. To speed up the solution exchange from dopamine 100 µM to PBS, the liquid was manually removed and replaced with fresh PBS (grey-coloured regions). As emphasized in Fig.4.19b, the current levels in PBS and dopamine solutions are not the same over time. This drifting behaviour in current could be related to the variation of the Ag/AgCl electrodes used as sensing and reference electrodes over time or to a partial etch of the quartz walls due to

the immersion in PBS solutions for long periods. Even with this drifting effect, the current variation between PBS and dopamine currents is evident.

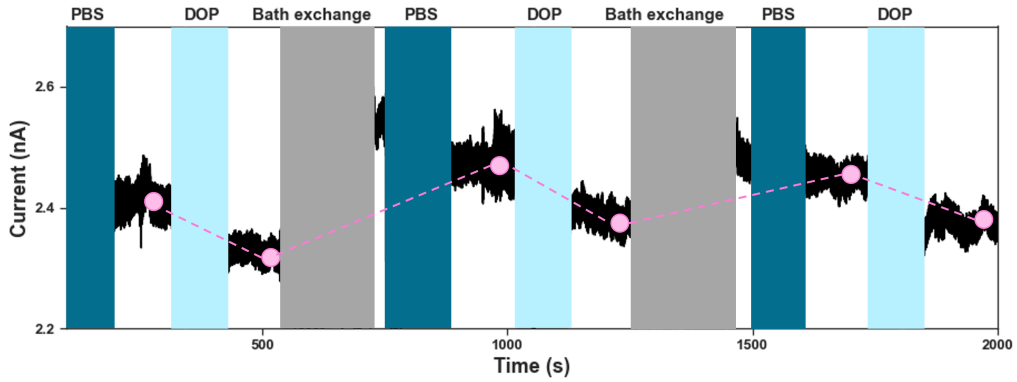

(a)

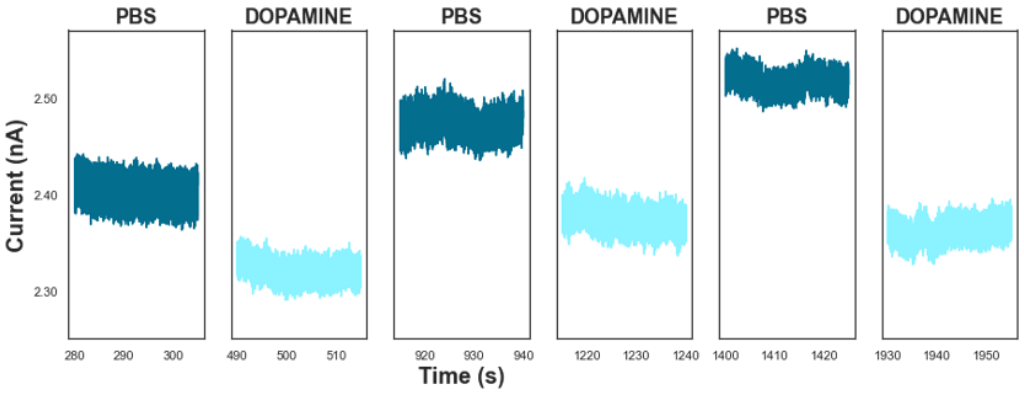

(b)

Figure 4.19: Multiple dopamine detection with real-time measurements. (a) Real-time recording with the different coloured regions related to the solution injection periods. PBS and dopamine 100 µM (DOP) are pumped in the mold. (b) Extraction from the real-time measurements to show the reaction magnitude and reset-ability. Time periods of 25 s for each bath.

Dopamine concentration dependence was interrogated in flow with PBS solutions (Fig.4.20a) and a calibration curve was extracted (Fig.4.20b). Dopamine concentration solutions from 1 fM to 100 µM were injected to derive the linear working region. Between 1 fM to 100 nM the sensor response appears linear and a current variation is already present at 1 fM dopamine concentration. This experiment was executed with one sensor, and repeating with other nanopipettes with a higher number of concentrations is needed to extract a reliable limit of detection and calibration curve.

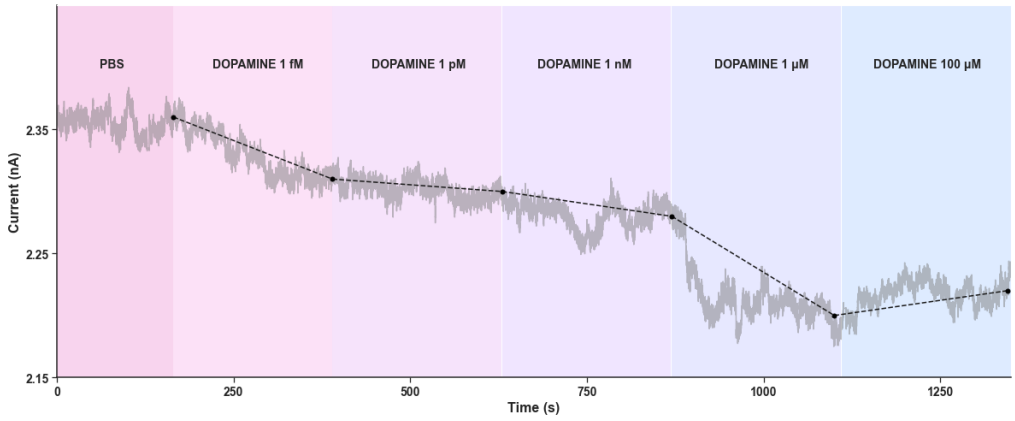

(a)

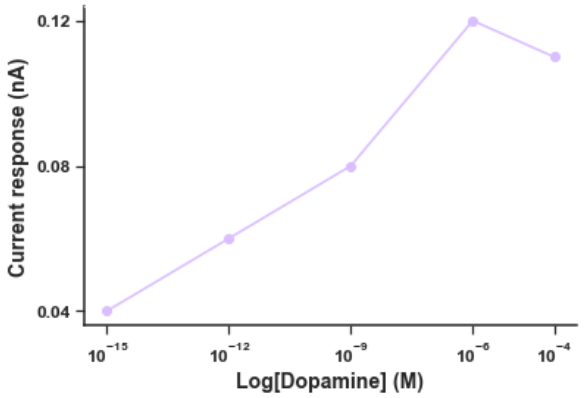

(b)

Figure 4.20: (a) Dopamine reaction at different concentrations in phosphate-buffered saline Calibration curve in flow for a dopamine aptamer-modified nanopipette. (b) Calibration curve obtained from the same experiment. [N=1]

Sensitive and selective dopamine sensors using this new polymer-based protocol to modify chemically glass nanopores have been developed. Various batches of single pore nanopipettes functionalized with biotinylated serotonin aptamers have been produced without promising results. The sensors did not react to serotonin at 100 µM concentration, even if the same protocol in the same environmental conditions was applied. The two aptamers show the same number of base pairs, but the main difference in the working principle between the two aptamers is given by the conformational change upon binding. Upon target detection, thiolated serotonin aptamers unfold and extend, while thiolated dopamine aptamers fold and shorten. The hypothesis is related to the inability to detect the current variation upon aptamer extension due to the packed layer-by-layer functionalization. Further analysis and investigations should be completed to understand the reason behind the non-reactivity to serotonin.

4.3.2 Double pore nanopipettes

Double pore nanopipettes were functionalized with this new PLL-g-PEG-based protocol. This protocol applied to double pore nanopipettes consists in functionalizing the sensor pore while leaving the control pore empty, and, when the sensor pore is completely functionalized, the control pore is aptamer-modified while leaving the sensor pore filled with PBS. Before moving to the functionalization of both pores with two different aptamers, the sensor pore was functionalized, while the control pore was left empty. Current-voltage recording (Fig.4.21) shows a significant difference in rectification: the functionalized sensor pore (dark blue curve) exhibits an higher rectification than the empty control pore (purple curve) that is bare quartz.

The next step from this positive result is functionalizing both pores with two distinctive aptamers: the dopamine-specific aptamers and the control sequence. To validate this functionalization protocol various measurement set-ups were used. For the manual bath exchange and the in flow measurements with one sensing electrode, the pores' response was not recorded simultaneously: the sensor pore was measured before the control pore.

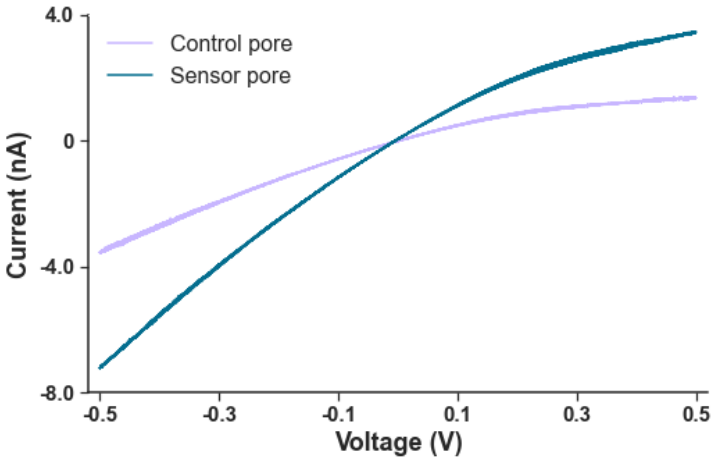

Figure 4.21: Current-voltage measurement of the sensor pore and control pore (empty) after the functionalization with the PLL-g-PEG-based protocol.

With the manual bath exchange set-up $N = 2$ nanopipettes worked as expected (Fig.4.22) where the sensor showed a current variation upon dopamine binding in the predicted range and a reset current when placed in PBS, while the control pore exhibits a constant current in the three baths. A similar good result with $N = 2$ double pore nanopipettes was obtained with the in flow recordings (Fig.4.23). In the shown example, the sensor pore did not reset the current to the initial baseline value, but the current modification upon the injection of the dopamine solution is $\sim 0.3\,\mathrm{nA}$ and not present in the control pore. Measuring the two pores in two different moments is the main limitation of these set-ups. Since the sensor pore is always experiencing the three solutions (PBS, dopamine and PBS) before the control

pore, a first possible dopamine reaction in the control pore may not be recorded. Being able to record the pores' response at the same time would prove the feasibility of this PLL-g-PEG-based protocol to double pore nanopipettes.

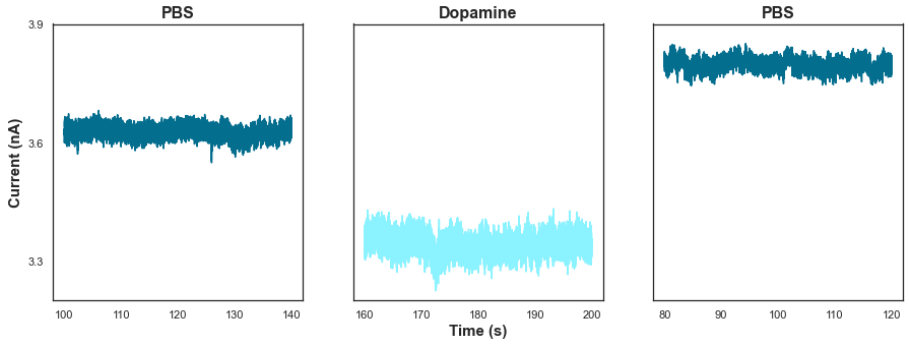

(a)

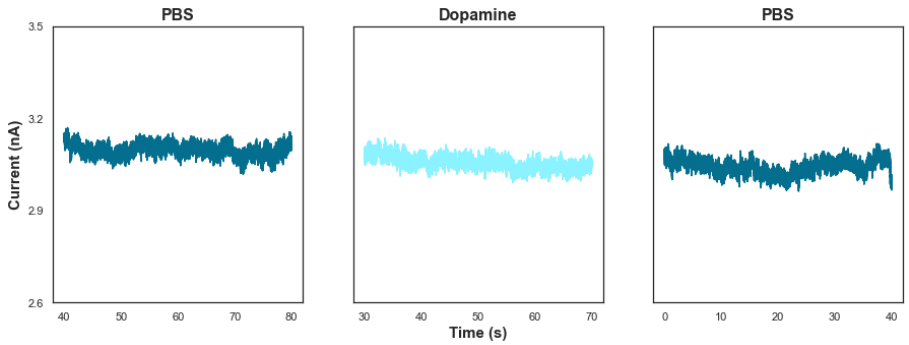

(b)

Figure 4.22: Current-time measurements with manual bath exchange set-up. (a) Sensor pore recording. (b) Control pore recording.

In the last measurement set-up, a second sensing electrode with a separate amplifier was added to the in flow set-up to allow the recording of both pores. For various nanopipettes, a mirrored current behaviour was observed between the two measured currents: when one pore was experiencing an increased drifty current, the other pore was facing a similar drift in the other direction. This unusual behaviour is related to the formation of a liquid bridge at the end of the nanopipette where the electrodes are inserted. This liquid bridge was connecting the two pores leading to opposite behaviour since the two pores act like two parallel resistors. The liquid connection was not constantly forming but was unavoidable for many nanopipettes. This behaviour leads to incomprehensible results where the current response upon dopamine binding was not clear. A possible solution is waxing the end where electrodes were inserted. This solution was not adequate for all nanopipettes because the quartz needs to be completely dry before the waxing step; otherwise, the wax is placed above the liquid, and the liquid bridge is formed.

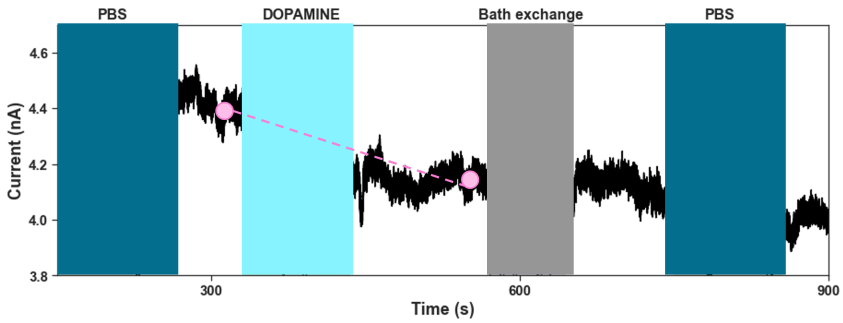

(a)

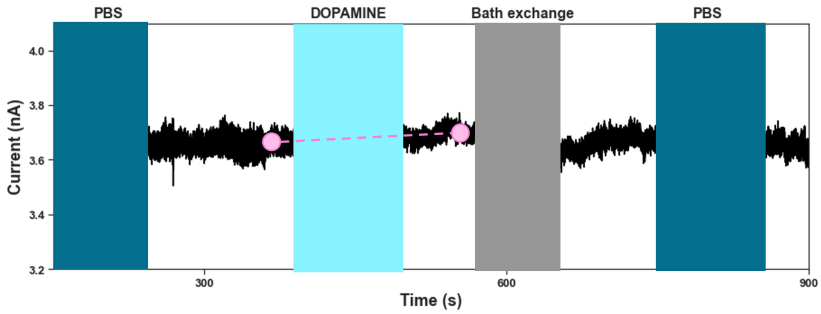

(b)

Figure 4.23: Current-time measurements in flow. (a) Sensor pore recording. (b) Control pore recording.

In Fig.4.24 the recording of an unwaxed nanopipette is proposed. This measurement set-up is noisier than the other suggested ones as noticeable in the recordings. The sensor pore shows a dopamine reaction after the solution injection, while the control pore exhibits a stable current over the injections. This first promising result needs to be further investigated.

Cross-contamination does not seem to play a central role in this functionalization protocol. Due to its more significant dimensions, the streptavidin-aptamer complex may be less likely to transverse pores at the tip. From the simultaneous measurements of the two pores with two sensing electrodes, a liquid bridge is present at the nanopipettes' end, but this liquid connection between the two pores does not appear to impact the overall functionalization.

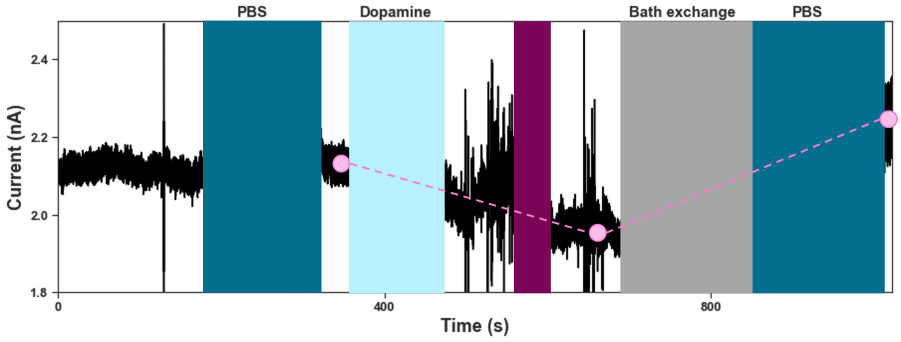

(a)

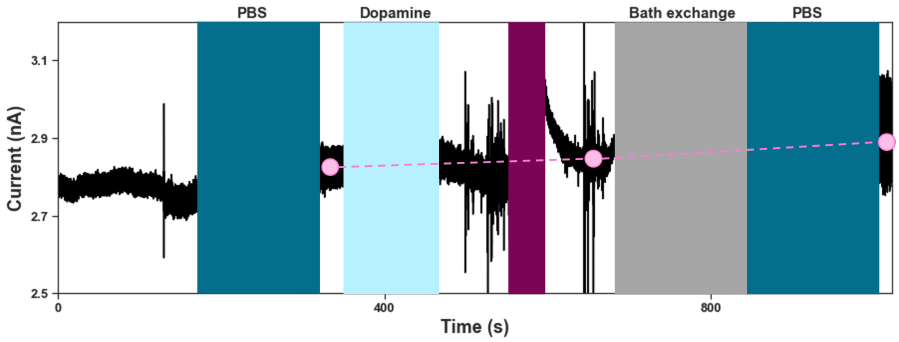

(b)

Figure 4.24: Current-time measurements in flow with one electrode in each pore. (a) Sensor pore recording. (b) Control pore recording.

4.3.3 Understanding surface binding through complementary techniques

Working principles

The multi-layer functionalization is evaluated with a combination of quartz crystal microbalance with dissipation monitoring (QCM-D) and optical waveguide lightmode spectroscopy (OWLS) to characterize the binding properties of aptamers using polymer-based surface chemistry. Hydration, viscoelastic properties, thickness and adsorbed mass on the surface are extracted from the recorded data. These two techniques are label-free biosensors with real-time measurements suited for the *in situ* measurement of the surface immobilization of biomolecules in an aqueous environment. These biosensors allow performing analysis from different aspects: from QCM-D the adsorbed mass includes the bound water molecules to the receptors and on the surface, while with OWLS, the dry mass is measured. From this information, the amount of bound water can be extracted.[61]

The optical waveguide lightmode spectroscopy is an optical biosensor based on the measurement of refractive index change originating from the presence of analytes

on the waveguide surface. Laser light is coupled into a waveguide thanks to a grating, and, under conditions of total internal reflection, light can only move across the waveguide and be detected at the photodiode when constructive interference occurs (Fig.4.25).[62][63] Constructive interference angles (α) are sensitive to changes in refractive index (N) according to:

$$N = n \sin \alpha + l \frac{\lambda}{\Lambda} \tag{4.1}$$

where n is the refractive index of covering medium, λ the laser wavelength, Λ the grating constant and l the diffraction order.[62][63]

Optical waveguide lightmode spectroscopy is sensitive to refractive index variations of the film compared to the aqueous background and, since the bound water molecules are not visible, the dry mass of the structure is obtained.[64] The main applications are *in situ* monitoring of macromolecules adsorption-desorption and adhesion of living cells onto a surface.[61]

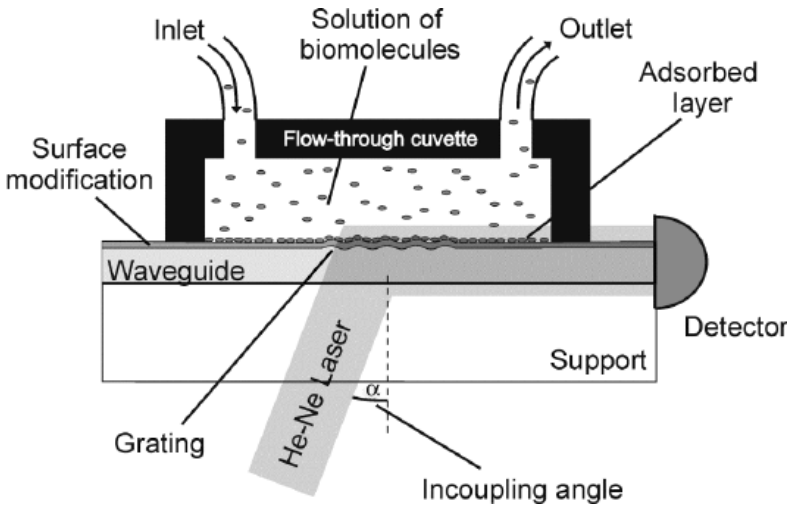

Figure 4.25: Schematic diagram of OWLS setup.[65]

Quartz crystal microbalance with dissipation monitoring is a mechanical, surface-sensitive, label-free biosensor that measures the shift in resonance frequency and the damping of the crystal oscillation (the dissipation factor) when the analyte binds to the surface. Information about hydrated mass, layer thickness and viscoelastic properties of the layers can be derived.[66] A piezoelectric chip is excited to its resonance by the application of an alternating voltage and resonant frequency and dissipation are recorded. The sensors have typically a diameter of 14 mm, a thickness of $\sim$ 300 µm, and a fundamental resonance frequency of 5 MHz.[61] The QCM-D chip is typically coated with metals on the top and bottom faces as the interface for the electrodes and an experimental substrate can be deposited (*e.g.* SiO_2). The 3^{rd}, 5^{th}, 7^{th}, 9^{th} and 11^{th} overtones are recorded simultaneously.[64]

The dissipation, linked to the mechanical properties of the analyte, is measured by the ring-down method measuring the decay of the oscillation after the excitation stops. From changes in the dissipation factor, the viscoelastic properties of the molecular assembly are derived as shown in Fig.4.26. As a first approximation, a significant dissipation variation is linked to a softer film. A shift in the resonant frequency reveals a mass variation: a decrease in resonance frequency reflects an increase in mass.[61] The mass derived from the Voigt model includes coupled water molecules (hydrated mass) since the frequency shift is sensitive to the bound water molecules on the surface.[61] The hydrated mass gives details about the structural changes of the arrangement even if the molecular mass remains constant. Thus, QCM-D enables detection of conformational changes of aptamers. The hydrated mass (m^{QCM}) can be described as

$$m^{QCM} = m_o + m_a \tag{4.2}$$

where m_o is the molecular mass and m_a is the coupled ambient solvent mass.[61]

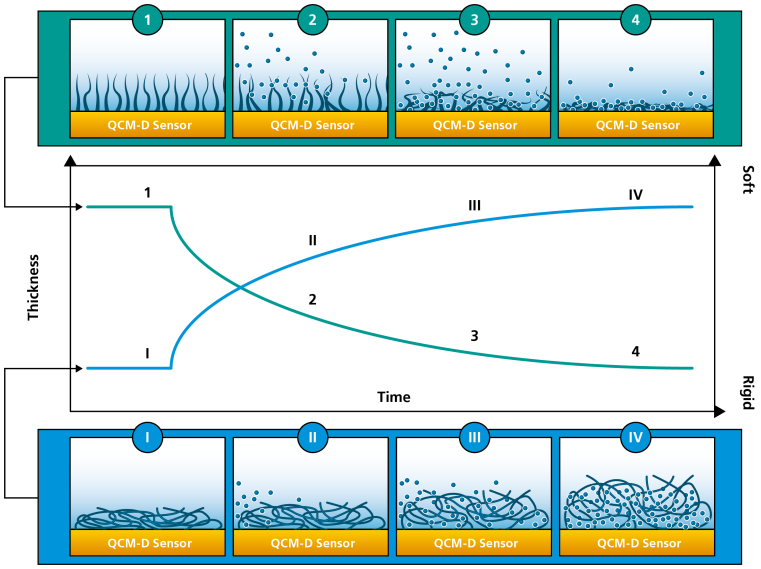

Figure 4.26: A schematic illustration of structural change as measured with QCM-D. The thickness is varying depending on the structural changes. (top) the molecules are bound to the solvent and, then, the molecules collapse releasing the coupled solvent. (bottom) the film is changing its mechanical properties from thin and rigid to thick and soft.[67]

To extract the adsorbed mass and the layer thickness from QCM-D recordings two models are typically used: the Sauerbrey equation and the Voigt viscoelastic model. The Sauerbrey equation is relating the change in frequency (Δf) with the mass variation (Δm) with a linear equation:[68]

$$\Delta m = -C * \frac{1}{n} * \Delta f \tag{4.3}$$

where n is the overtone number and C is a constant that depends on the sensor ($C \sim 17.7\,\mathrm{ng\,cm^{-2}\,Hz^{-1}}$ for quartz sensor at room temperature). This equation assumes that the small mass variation could be considered as a mass change of the crystal itself. The mass needs to be rigidly adsorbed on the surface. Another limitation is the assumption that the mass is evenly distributed over the sensor active area. This linearity between frequency and mass fails for viscoelastic films where the dissipation is theoretically zero.[61]

Fitting the frequency and the dissipation responses to a viscoelastic model gives details about the properties of the adsorbed film. The Voigt viscoelastic model is commonly used and consists of a (viscous) dashpot and (elastic) spring in parallel. Frequency and dissipation variation can be related to the adsorbed film viscoelastic properties and bulk solution properties:[69]

$$\Delta f \approx \frac{-1}{2\pi\rho_0\delta_0}\{(\frac{\eta_3}{\delta_3}) + \delta_1\rho_1\omega - 2\delta_1(\frac{\eta_3}{\delta_3})^2(\frac{\eta_1\omega^2}{\mu_1^2} + \omega^2 + \eta_1^2)\} \tag{4.4}$$

$$\Delta D \approx \frac{1}{\pi f\rho_0\delta_0}\{(\frac{\eta_3}{\delta_3}) + 2\delta_1(\frac{\eta_3}{\delta_3})^2(\frac{\eta_1\omega}{\mu_1^2} + \omega^2 + \eta_1^2)\} \tag{4.5}$$

ρ_0 and δ_0 are the density and thickness of the quartz crystal, η_3 is the viscosity of the bulk liquid, δ_3 is the viscous penetration depth of the shear wave in the bulk liquid, and ω is the angular frequency. ρ_1, η_1, μ_1 and δ_1 are the density, viscosity, shear elasticity and thickness of the adsorbed layer and these parameters are unknowns. To fit the obtained measurements from QCM-D at least two overtones of the fundamental frequencies are needed.[69]

Comparing the mass densities obtained from QCM-D (m^{QCM}) and OWLS (m^{OWLS}) the amount of bound water (m_W) and the hydration degree (φ) with respect to the wet mass can be extracted. The mass of bound water is simply the difference between the wet mass and dry mass, while the hydration degree can be calculated as:[61]

$$\varphi = \frac{m^{QCM} - m^{OWLS}}{m^{QCM}} * 100 \tag{4.6}$$

Assembled layer monitoring and target binding

The main questions to address with QCM-D and OWLS results are related to the effective binding of the assembled layer, the dopamine aptamer-target binding, thicknesses and masses of the layers and the hydration degree.

In Fig.4.27 the recorded frequency variation for the assembly of the layer-by-layer functionalization through QCM-D is shown. The coloured regions refer to the injection and incubation time of various solutions and the white areas for the baseline and rinsing times with PBS. The first jump (purple section) in frequency is related to the assembly of the PLL-g-PEG monolayer, while the second jump (pink section) to the streptavidin-aptamer complex. The streptavidin-aptamer complex section required a wider time range and more injections to reach mass saturation

while PLL-g-PEG interaction with the quartz surface is faster. During the PBS rinses the frequency, and so the adsorbed mass, should be stable over time without losses as in Fig.4.27. The same experiment has been repeated $N = 3$ times with high reproducibility. This result is addressing the effective binding of the layer-by-layer functionalization.

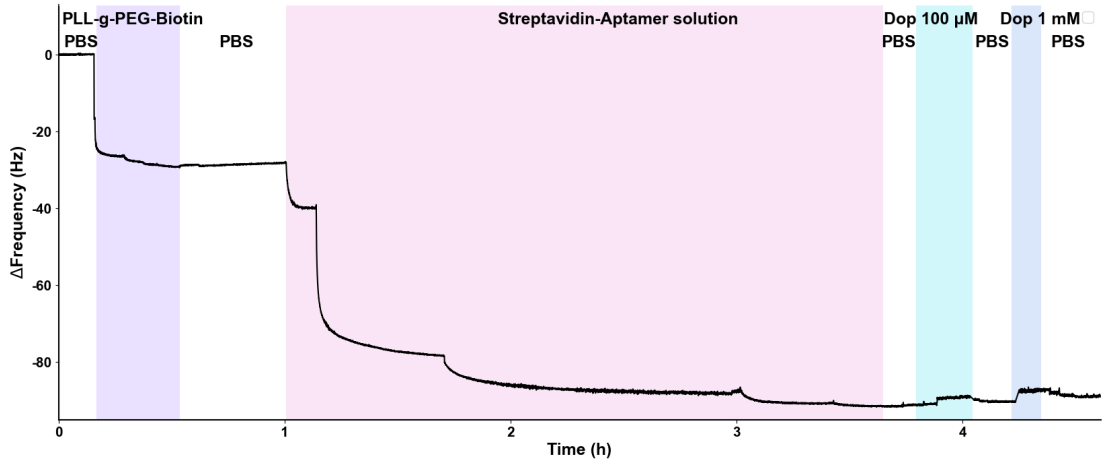

Figure 4.27: On a SiO_2 surface a monolayer of PLL-g-PEG with 15% biotin is assembled and then the streptavidin-aptamer complex is binding on top of PLL-g-PEG. After every mass saturation with a new layer, various rinsing with PBS are performed to show the permanent binding on the surface. Frequency variation upon injection of 1 mM and 100 µM Dopamine are present.

The second question to tackle is the binding of dopamine molecules to aptamers. This second aspect is analyzed through QCM-D after the assembly of the layer-by-layer functionalization (Fig.4.27). In Fig.4.28a and Fig.4.28b the dopamine binding is investigated as variation in the frequency and dissipation of the dopamine aptamer and control sequence when 1 mM dopamine solution is injected. Upon injection of dopamine solution, the aptamer binding is revealed with a positive frequency variation of ~ 2 Hz, while the control sequence shows a weaker frequency variation and a stable dissipation response. Dopamine solutions have been injected multiple times to saturate the variation. When PBS is introduced, dopamine molecules are released from the aptamers and the response is going back to the baseline for frequency and dissipation. This result verifies the binding and reset properties of dopamine aptamers.

In Fig.4.28c multiple dopamine detection and releases are shown. Even with an unstable baseline, the frequency shift upon dopamine binding and release are evident. In Table 4.1 the extracted frequency shifts of PLL-g-PEG and streptavidin-aptamer complex assembly and dopamine binding. The standard error of the mean for the streptavidin-aptamer complex is significant because the frequency shift is dependent on the previously bound amount of PLL-g-PEG on the chip.

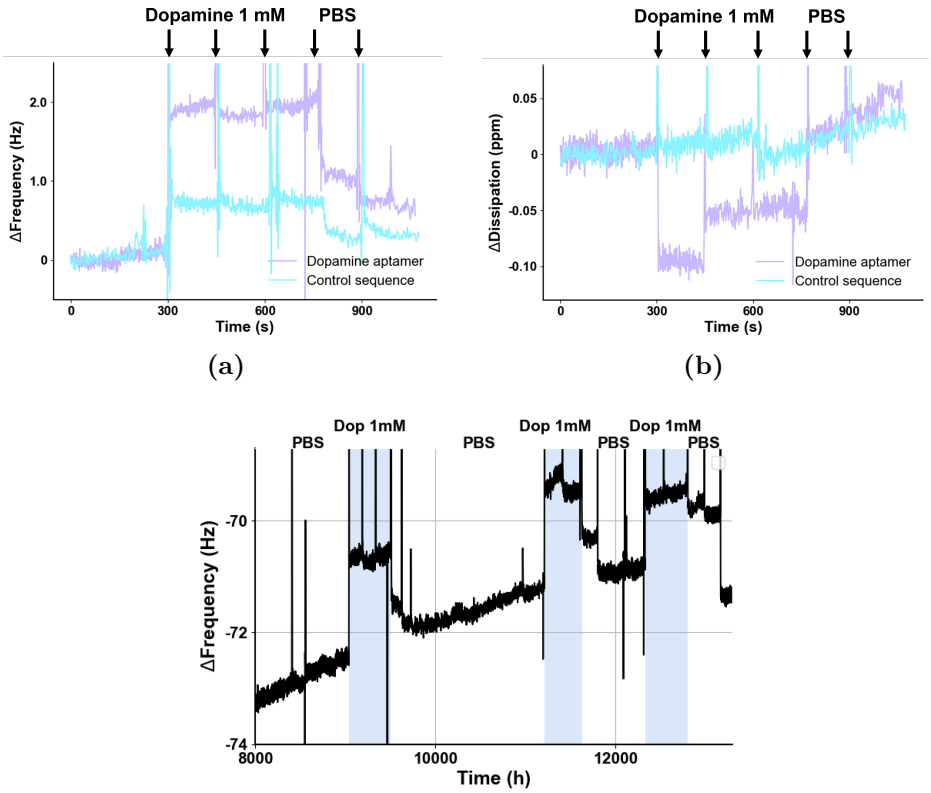

Figure 4.28: Characterization of the binding mechanism of dopamine aptamers through QCM-D. (a)(b) An increase in frequency and decrease in dissipation upon dopamine addition reveals the ability of dopamine aptamers to bind to dopamine. A variation in the dissipation shows the typical conformation change of aptamer. The binding of dopamine aptamers is reversible since the frequency is going back to the baseline value when phosphate-buffered saline (PBS) is injected. A control sequence was analyzed and a minimum frequency and dissipation variation can be noticed. The arrows indicate the injection times. (c) Multiple aptamer binding and release. The blue-coloured regions are the intervals when the chip was in contact with the dopamine solution.

PLL-g-PEG	$22.7 \pm 2.9\,\mathrm{Hz}$	$N = 3$
Streptavidin-aptamer complex	$49.2 \pm 9.1\,\mathrm{Hz}$	$N = 3$
Dopamine reaction	$\sim 2 - 2.5\,\mathrm{Hz}$	$N = 4$

Table 4.1: Obtained frequency shifts when the layers were binding and upon dopamine reaction and the number of repetitions. For PLL-g-PEG and streptavidin-aptamer complex the mean and standard error of the man are shown.

From OWLS the dry absorbed mass of the functionalization assembled layers is recorded (Fig.4.29). The assembly of PLL-g-PEG and streptavidin-aptamer complex can be analyzed while the aptamer-target binding is not observed. The dopamine molecules have a small dry mass to be detected with this technique, while with the QCM-D technique the conformational change is taken into account. Experiments were performed with OWLS to evaluate the dry mass of the layer-by-layer functionalization and to verify the effective binding of the functionalization layer with a different technique than QCM-D.

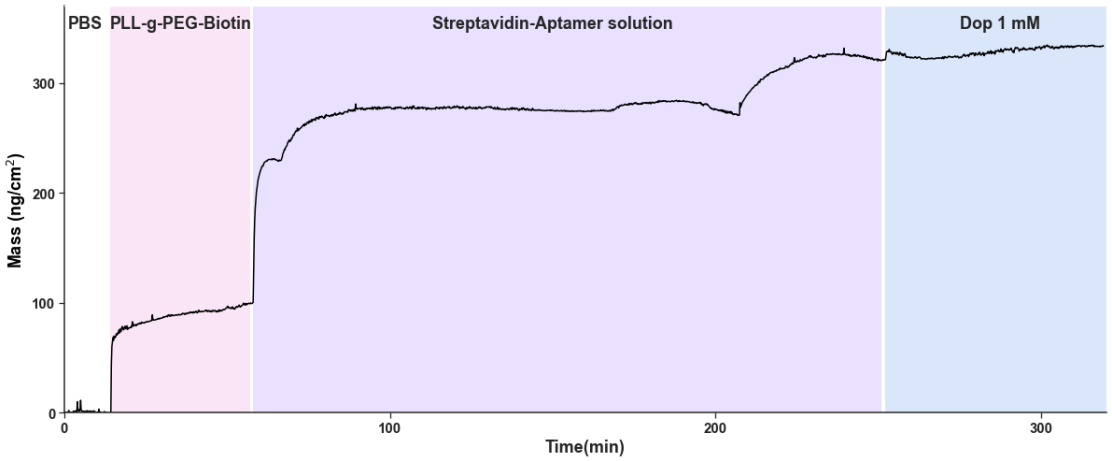

Figure 4.29: On a SiO_2 surface a monolayer of PLL-g-PEG with 15% biotin is assembled and then the streptavidin-aptamer complex is binding on top of PLL-g-PEG. After every mass saturation with a new layer, various rinsing with PBS are performed to show the permanent binding on the surface. No mass variation can be noticed when 1 mM Dopamine is injected.

In Fig4.30 the dry and wet mass variations are compared over time. The difference between the two curves reveals the bound water molecules in the assembled layers. In both cases, there is a jump in mass every time a new layer is injected. In Fig.4.30a multiple mass recordings are compared ($N \geq 2$). The dry masses obtained from OWLS are consistent over different experiments.

The thickness of the various elements of the functionalization is derived from the Voigt viscoelastic model since the layer-by-layer functionalization is not considered as a rigid absorption (Fig.4.30c). The derived thickness values are coherent with literature: PLL-g-PEG is ~ 6 nm[55] and the streptavidin-aptamer complex ~ 10 nm where the streptavidin is 4.2 nm by 4.2 nm by 5.6 nm[70] and aptamers are ~ 5 nm[31]. With the same fitting model, the wet adsorbed mass is evaluated from frequency shifts and dissipation variations (Fig.4.30c).

Complementing the QCM-D results with OWLS measurements leads to the extraction of the hydration degree of the examined layers. From Fig.4.30a the

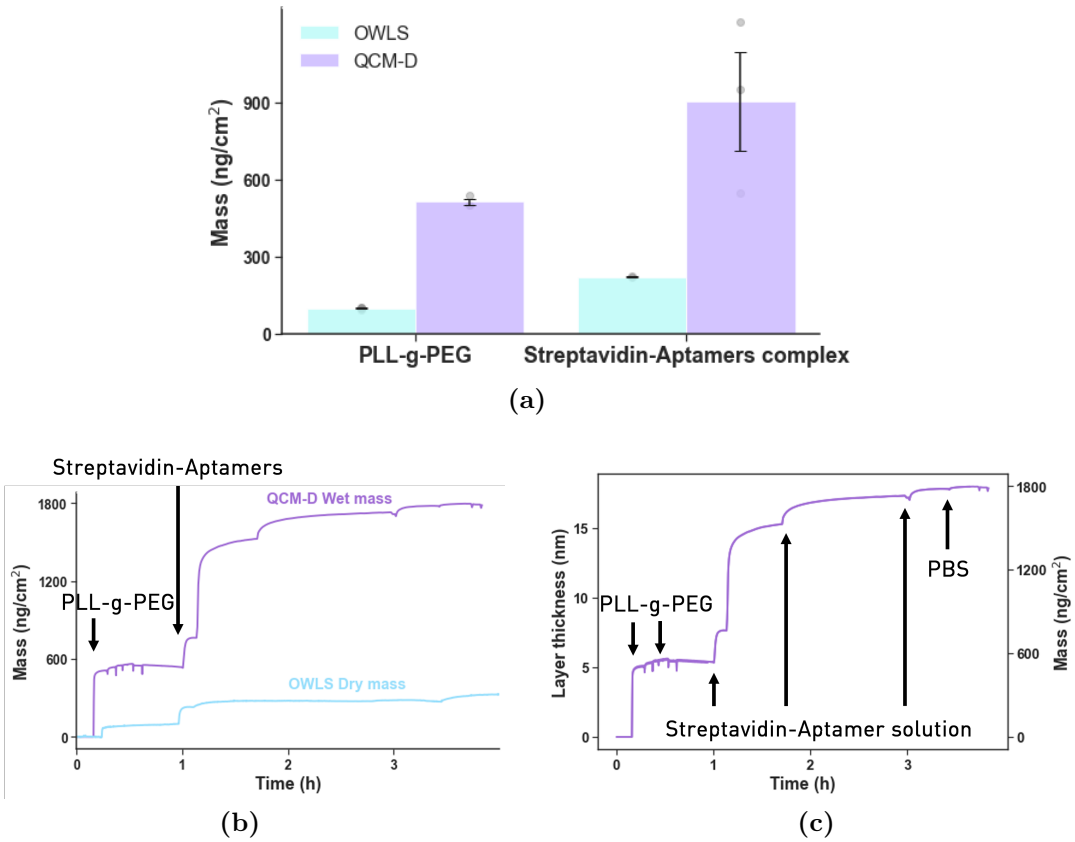

Figure 4.30: Parameters extraction from QCM-D and OWLS analysis. (a) Comparison between the mass values obtained from QCM-D and OWLS analysis. The dry mass value is extracted from OWLS, while the wet mass from QCM-D. The mean and the standard error of the mean are depicted. (b) Wet and dry mass comparison in real-time when PLL-g-PEG and streptavidin-aptamer complex are injected. (c) Thickness and wet mass of the functionalization layers from Voigt model interpolation.

hydration degree (φ) is evaluated using Eq.4.6 for PLL-g-PEG and streptavidin-aptamer layer. The hydration degree of PLL-g-PEG is $\sim 81\%$ with a bound water mass of $\sim 420\,\mathrm{ng\,cm^{-2}}$. The results are in line with literature where the water content is shown to be in the range $80 - 84\%$.[68][71] Streptavidin-aptamer complex exhibits an hydration degree of $\sim 75\%$ with a bound water mass of $\sim 680\,\mathrm{ng\,cm^{-2}}$.

Chapter 5

Conclusions and outlook

An alternative functionalization protocol to produce sensitive and selective aptamer-modified quartz nanopipettes to detect dopamine has been developed. The combination of nanopipettes with dopamine aptamers confers high spatial resolution with high specificity and selectivity for dopamine detection. The nanoscale pore allows recording of the ion flux variation induced by aptamers' conformation change upon target binding thanks to the ion current rectification effect. Surface-sensitive techniques, such as quartz crystal microbalance with dissipation and optical waveguide lightmode spectroscopy, enable the characterization of the assembled layers.

The developed aptamer-modified nanopipettes demonstrated selective responses with high concentrations of interferents such as norepinephrine and levodopa. Sensors enable the detection of dopamine multiple times in flow thanks to the reset-ability of aptamers revealing the possibility to be applied for *in vitro* and *ex-vivo* experiments.

Furthermore, the sensing platform was modified from single pore nanopipettes to double pore to enable multiplexed sensing. With the polymer-based chemistry, the functionalization of the two pores with the dopamine aptamer and the control sequence was examined in flow with promising results. Further experiments with the simultaneous recording of the two pores are essential to prove ultimately the absence of cross-contamination. Double pore nanopipettes allow self-referencing measurements and open the possibility to investigate the functionalization with two sensor aptamers to perform the detection of multiple target analytes at the same time and in the same location.

Further investigation about the limit of detection and dopamine detection in complex media is needed to complete the validation of double pore nanopipettes for dopamine detection. Double pore nanopipettes are promising to perform multiplexed biosensing of neurochemical flux in close proximity to synapses of *in vitro* neural networks and *ex-vivo* experiments with brain slices.

References

[1] S. E. Hyman, «Neurotransmitters», *Current Biology*, vol. 15, no. 5, R154–R158, 2005. DOI: 10.1016/j.cub.2005.02.037 (cit. on p. 1).

[2] K. Sukel, *Neurotransmitters*. [Online]. Available: https://www.dana.org/article/neurotransmitters, Accessed: 11.05.2022 (cit. on p. 1).

[3] C. Hammond and M. Esclapez, «Chapter 6 - the chemical synapses», in *Cellular and Molecular Neurophysiology (Fourth Edition)*, Academic Press, 2015, pp. 121–144. DOI: 10.1016/B978-0-12-397032-9.00006-6 (cit. on p. 1).

[4] L. S. P. Zachary M. Sheffler Vamsi Reddy, *Physiology, Neurotransmitters*. StatPearls Publishing, 2021 (cit. on p. 2).

[5] *Neurotransmitters*, Accessed on 23.08.2022. [Online]. Available: https://my.clevelandclinic.org/health/articles/22513-neurotransmitters (cit. on p. 2).

[6] N. Thakur, D. Gupta, D. Mandal, and T. C. Nagaiah, «Ultrasensitive electrochemical biosensors for dopamine and cholesterol: Recent advances, challenges and strategies», *Chem. Commun.*, vol. 57, pp. 13 084–13 113, 97 2021. DOI: 10.1039/D1CC05271C (cit. on p. 2).

[7] L. Speranza, U. di Porzio, D. Viggiano, A. de Donato, and F. Volpicelli, «Dopamine: The neuromodulator of long-term synaptic plasticity, reward and movement control», *Cells*, vol. 10, no. 4: 735, 2021. DOI: 10.3390/cells10040735 (cit. on pp. 2, 3).

[8] P. B. Foley, «Dopamine in psychiatry: A historical perspective», *Journal of Neural Transmission*, vol. 126, no. 4, pp. 473–479, 2019. DOI: 10.1007/s00702-019-01987-0 (cit. on p. 2).

[9] S. Lakard, I.-A. Pavel, and B. Lakard, «Electrochemical biosensing of dopamine neurotransmitter: A review», *Biosensors*, vol. 11, no. 6, 2021. DOI: 10.3390/bios11060179 (cit. on pp. 2, 3).

[10] S. Basu and P. S. Dasgupta, «Dopamine, a neurotransmitter, influences the immune system», *Journal of Neuroimmunology*, vol. 102, no. 2, pp. 113–124, 2000. DOI: 10.1016/S0165-5728(99)00176-9 (cit. on p. 3).

[11] C. Sarkar, B. Basu, D. Chakroborty, P. S. Dasgupta, and S. Basu, «The immunoregulatory role of dopamine: An update», *Brain, Behavior, and Immunity*, vol. 24, no. 4, pp. 525–528, 2010. DOI: 10.1016/j.bbi.2009.10.015 (cit. on p. 3).

[12] N. Thakur, D. Gupta, D. Mandal, and T. C. Nagaiah, «Ultrasensitive electrochemical biosensors for dopamine and cholesterol: Recent advances, challenges and strategies», *Chemical Communications*, vol. 57, pp. 13 084–13 113, 2021. DOI: 10.1039/D1CC05271C (cit. on pp. 3, 4).

[13] X. Liu and J. Liu, «Biosensors and sensors for dopamine detection», *VIEW*, vol. 2, no. 1, p. 20 200 102, 2021. DOI: 10.1002/VIW.20200102 (cit. on pp. 3–5).

[14] H. Gu, E. Varner, S. Groskreutz, A. Michael, and S. Weber, «In vivo monitoring of dopamine by microdialysis with one-minute temporal resolution using online capillary liquid chromatography with electrochemical detection», *Analytical chemistry*, vol. 87, pp. 6088–6094, 2015. DOI: 10.1021/acs.analchem.5b00633 (cit. on p. 3).

[15] S. Lakard, I.-A. Pavel, and B. Lakard, «Electrochemical biosensing of dopamine neurotransmitter: A review», *Biosensors*, vol. 11, p. 179, 2021. DOI: 10.3390/bios11060179 (cit. on pp. 3, 4).

[16] C. He, M. Tao, C. Zhang, Y. He, W. Xu, Y. Liu, and W. Zhu, «Microelectrode-based electrochemical sensing technology for in vivo detection of dopamine: Recent developments and future prospects», *Critical Reviews in Analytical Chemistry*, vol. 52, pp. 1–11, 2020. DOI: 10.1080/10408347.2020.1811946 (cit. on pp. 3, 4).

[17] S. Casalini, F. Leonardi, T. Cramer, and F. Biscarini, «Organic field-effect transistor for label-free dopamine sensing», *Organic Electronics*, vol. 14, pp. 156–163, 2012. DOI: 10.1016/j.orgel.2012.10.027 (cit. on pp. 4, 5).

[18] C. Zhao, K. Cheung, I.-W. Huang, H. Yang, N. Nakatsuka, W. Liu, Y. Cao, T. Man, P. Weiss, H. Monbouquette, and A. Andrews, «Implantable aptamer-field-effect transistor neuroprobes for in vivo neurotransmitter monitoring», *Science advances*, vol. 7, p. 7422, 2021. DOI: 10.1126/sciadv.abj7422 (cit. on p. 4).

[19] F. Kamal Eddin and Y. W. Fen, «Recent advances in electrochemical and optical sensing of dopamine», *Sensors*, vol. 20, p. 47, 2020. DOI: 10.3390/s20041039 (cit. on p. 5).

[20] J. Stanley and N. Pourmand, «Nanopipettes - the past and the present», *APL Materials*, vol. 8, p. 100 902, 2020. DOI: 10.1063/5.0020011 (cit. on pp. 5, 6, 16, 17).

[21] Y. Wang, D. Wang, and M. Mirkin, «Resistive-pulse and rectification sensing with glass and carbon nanopipettes», *Proceedings of the Royal Society A: Mathematical, Physical and Engineering Science*, vol. 473, p. 20 160 931, 2017. DOI: 10.1098/rspa.2016.0931 (cit. on pp. 5, 16–18, 20).

[22] M. Chang, G. Morgan, F. Bedier, A. Chieng, P. Gomez, S. Raminani, and Y. Wang, «Review—recent advances in nanosensors built with pre-pulled glass nanopipettes and their applications in chemical and biological sensing», *Journal of The Electrochemical Society*, vol. 167, p. 037 533, 2020. DOI: 10.1149/1945-7111/ab64be (cit. on pp. 5, 6, 17).

[23] K. Kececi, A. Dinler, and D. Kaya, «Review—nanopipette applications as sensors, electrodes, and probes: A study on recent developments», *Journal of The Electrochemical Society*, vol. 169, no. 2, p. 027 502, 2022. DOI: 10.1149/1945-7111/ac4e58 (cit. on pp. 5, 6, 16, 18–20).

[24] M. H. Ali, M. E. Elsherbiny, and M. Emara, «Updates on aptamer research», *International Journal of Molecular Sciences*, vol. 20, no. 10, 2019. DOI: 10.3390/ijms20102511 (cit. on pp. 6–9).

[25] H. Sun and Y. Zu, «A highlight of recent advances in aptamer technology and its application», *Molecules*, vol. 20, no. 7, pp. 11 959–11 980, 2015. DOI: 10.3390/molecules200711959 (cit. on pp. 6–8).

[26] E. Cho, J.-W. Lee, and A. Ellington, «Applications of aptamers as sensors», *Annual review of analytical chemistry (Palo Alto, Calif.)*, vol. 2, pp. 241–64, 2009. DOI: 10.1146/annurev.anchem.1.031207.112851 (cit. on pp. 6, 7).

[27] Adachi and Nakamura, «Aptamers: A review of their chemical properties and modifications for therapeutic application», *Molecules*, vol. 24, p. 4229, 2019. DOI: 10.3390/molecules24234229 (cit. on pp. 7, 8).

[28] N. Nakatsuka, K.-A. Yang, J. M. Abendroth, K. M. Cheung, X. Xu, H. Yang, C. Zhao, B. Zhu, Y. S. Rim, Y. Yang, P. S. Weiss, M. N. Stojanović, and A. M. Andrews, «Aptamer-field-effect transistors overcome debye length limitations for small-molecule sensing», *Science*, vol. 362, no. 6412, pp. 319–324, 2018. DOI: 10.1126/science.aao6750 (cit. on pp. 7, 11, 20, 31).

[29] *Selex*, Accessed on 03.08.2022. [Online]. Available: https://2018.igem.org/Team:Madrid-OLM/AptDiscovery (cit. on p. 7).

[30] M. Bauer, M. Strom, D. S. Hammond, and S. Shigdar, «Anything you can do, i can do better: Can aptamers replace antibodies in clinical diagnostic applications?», *Molecules*, vol. 24, no. 23, 2019. DOI: 10.3390/molecules24234377 (cit. on p. 8).

[31] N. Nakatsuka, A. Faillétaz, D. Eggemann, C. Forro, J. Vörös, and D. Momotenko, «Aptamer conformational change enables serotonin biosensing with nanopipettes», *Analytical Chemistry*, vol. 93, pp. 4033–4041, 2021. DOI: 10.1021/acs.analchem.0c05038 (cit. on pp. 10, 11, 24, 37, 54).

[32] T. Jäggi, «Towards multiplexed sensing using aptamer-modified nanopipette», M.S. thesis, ETH, 2021 (cit. on pp. 10, 11, 23, 24, 29).

[33] X. Du, L. Li, J. Li, C. Yang, N. Frenkel, A. Welle, S. Heissler, A. Nefedov, M. Grunze, and P. A. Levkin, «Uv-triggered dopamine polymerization: Control of polymerization, surface coating, and photopatterning», *Advanced Materials*, vol. 26, no. 47, pp. 8029–8033, 2014. DOI: 10.1002/adma.201403709 (cit. on p. 13).

[34] X. Du, L. Li, F. Behboodi-Sadabad, A. Welle, J. Li, S. Heissler, H. Zhang, N. Plumeré, and P. A. Levkin, «Bio-inspired strategy for controlled dopamine polymerization in basic solutions», *Polym. Chem.*, vol. 8, pp. 2145–2151, 14 2017. DOI: 10.1039/C7PY00051K (cit. on p. 13).

[35] S. Zhang, M. Li, B. Su, and Y. Shao, «Fabrication and use of nanopipettes in chemical analysis», *Annual Review of Analytical Chemistry*, vol. 11, pp. 265–286, 2018. DOI: 10.1146/annurev-anchem-061417-125840 (cit. on pp. 16, 17).

[36] R.-J. Yu, Y.-L. Ying, R. Gao, and Y.-T. Long, «Confined nanopipette sensing: From single molecules, single nanoparticles, to single cells», *Angewandte Chemie International Edition*, vol. 58, no. 12, pp. 3706–3714, 2019. DOI: 10.1002/anie.201803229 (cit. on p. 16).

[37] Z. Siwy, «Ion-current rectification in nanopores and nanotubes with broken symmetry», *Advanced Functional Materials*, vol. 16, no. 6, pp. 735–746, 2006. DOI: 10.1002/adfm.200500471 (cit. on pp. 17–19).

[38] C. Wei, A. J. Bard, and S. W. Feldberg, «Current rectification at quartz nanopipet electrodes», *Analytical Chemistry*, vol. 69, no. 22, pp. 4627–4633, 1997. DOI: 10.1021/ac970551g (cit. on pp. 17–19, 31).

[39] X. Yin, S. Zhang, Y. Dong, S. Liu, J. Gu, Y. Chen, X. Zhang, X. Zhang, and Y. Shao, «Ionic current rectification in organic solutions with quartz nanopipettes», *Analytical Chemistry*, vol. 87, no. 17, pp. 9070–9077, 2015. DOI: 10.1021/acs.analchem.5b02337 (cit. on p. 18).

[40] D. Perry, D. Momotenko, R. A. Lazenby, M. Kang, and P. R. Unwin, «Characterization of nanopipettes», *Analytical Chemistry*, vol. 88, no. 10, pp. 5523–5530, 2016. DOI: 10.1021/acs.analchem.6b01095 (cit. on pp. 19, 20).

[41] M. Simonis and S. Hennig, «Preparation and loading of nanopipettes - tips & tricks for nanoinjection, nanodeposition and sicm», *Wiley Analytical Science Magazine*, 2017. DOI: 10.13140/RG.2.2.35563.69928 (cit. on p. 21).

[42] E. Salançon and B. Tinland, «Filling nanopipettes with apertures smaller than 50 nm: Dynamic microdistillation», *Beilstein Journal of Nanotechnology*, vol. 9, pp. 2181–2187, 2018. DOI: 10.3762/bjnano.9.204 (cit. on p. 21).

[43] L. Sun, K. Shigyou, T. Ando, and S. Watanabe, «Thermally driven approach to fill sub-10-nm pipettes with batch production», *Analytical Chemistry*, vol. 91, no. 21, pp. 14 080–14 084, 2019. DOI: 10.1021/acs.analchem.9b03848 (cit. on p. 21).

[44] P. Cadinu, G. Campolo, S. Pud, W. Yang, J. B. Edel, C. Dekker, and A. P. Ivanov, «Double barrel nanopores as a new tool for controlling single-molecule transport», *Nano Letters*, vol. 18, no. 4, pp. 2738–2745, 2018. DOI: 10.1021/acs.nanolett.8b00860 (cit. on pp. 22, 24, 30, 32).

[45] R. Ren, X. Wang, S. Cai, Y. Zhang, Y. Korchev, A. Ivanov, and J. Edel, «Selective sensing of proteins using aptamer functionalized nanopore extended field-effect transistors», *Small Methods*, vol. 4, p. 2 000 356, 2020. DOI: 10.1002/smtd.202000356 (cit. on p. 22).

[46] R. Ren, X. Wang, S. Cai, Y. Zhang, Y. Korchev, A. Ivanov, and J. Edel, «Selective sensing of proteins using aptamer functionalized nanopore extended field-effect transistors», *Small Methods*, vol. 4, p. 2 000 356, 2020. DOI: 10.1002/smtd.202000356 (cit. on p. 22).

[47] P. Cadinu, M. Kang, B. Nadappuram, A. Ivanov, and J. Edel, «Individually addressable multi-nanopores for single-molecule targeted operations», *Nano Letters*, vol. 40, no. 3, pp. 2012–2019, 2020. DOI: 10.1021/acs.nanolett.9b05307 (cit. on p. 22).

[48] Q. Liu, H. Wu, L. Wu, X. Xie, J. Kong, X. Ye, and L. Liu, «Voltage-driven translocation of dna through a high throughput conical solid-state nanopore», *PLOS ONE*, vol. 7, no. 9, pp. 1–9, 2012. DOI: 10.1371/journal.pone.0046014 (cit. on pp. 24, 32).

[49] N. Bell, K. Chen, S. Ghosal, M. Ricci, and U. Keyser, «Asymmetric dynamics of dna entering and exiting a strongly confining nanopore», *Nature Communications*, vol. 8: 380, 2017. DOI: 10.1038/s41467-017-00423-9 (cit. on pp. 29, 30, 32).

[50] R. Fraccari, M. Carminati, G. Piantanida, T. Leontidou, G. Ferrari, and T. Albrecht, «High-bandwidth detection of short dna in nanopipettes», *Faraday Discuss.*, vol. 193, pp. 459–470, 2016. DOI: 10.1039/C6FD00109B (cit. on pp. 30, 32, 34).

[51] R. Fraccari, P. Ciccarella, A. Bahrami, M. Carminati, G. Ferrari, and T. Albrecht, «High-speed detection of dna translocation in nanopipettes», *Nanoscale*, vol. 8, pp. 7604–7611, 2016. DOI: 10.1039/C5NR08634E (cit. on p. 30).

[52] M. F. Alawami, F. Bošković, J. Zhu, K. Chen, S. E. Sandler, and U. F. Keyser, «Lifetime of glass nanopores in a pdms chip for single-molecule sensing», *iScience*, vol. 25, no. 5, p. 104 191, 2022. DOI: 10.1016/j.isci.2022.104191 (cit. on p. 30).

[53] C. Wang, S. Sensale, Z. Pan, and S. Senapati, «Slowing down dna translocation through solid-state nanopores by edge-field leakage», *Nature Communications*, vol. 12: 140, 2021. DOI: 10.1038/s41467-020-20409-4 (cit. on p. 30).

[54] L. J. Steinbock, R. D. Bulushev, S. Krishnan, C. Raillon, and A. Radenovic, «Dna translocation through low-noise glass nanopores», *ACS nano*, vol. 7, no. 12, pp. 11 255–11 262, 2013. DOI: 10.1021/nn405029j (cit. on p. 32).

[55] S. S. TECHNOLOGY, *Susos pll-g-peg polymers*, Accessed on 01.07.2022. [Online]. Available: https://susos.com/beschichtungstechnologien/pll-g-peg-polymere/ (cit. on pp. 35, 37, 54).

[56] C. Feng, Y. Li, D. Yang, J. Hu, X. Zhang, and X. Huang, «Cheminform abstract: Well-defined graft copolymers: From controlled synthesis to multipurpose applications», *Chemical Society reviews*, vol. 40, pp. 1282–95, 2010. DOI: 10.1039/b921358a (cit. on p. 35).

[57] F. Liu, J. Zhang, and Y. Mei, «The origin of the cooperativity in the streptavidin-biotin system: A computational investigation through molecular dynamics simulations», *Scientific Reports*, vol. 6, p. 27 190, 2016. DOI: 10.1038/srep27190 (cit. on pp. 35, 36).

[58] A. Jain and K. Cheng, «The principles and applications of avidin-based nanoparticles in drug delivery and diagnosis», *Journal of Controlled Release*, vol. 245, pp. 27–40, 2016. DOI: 10.1016/j.jconrel.2016.11.016 (cit. on pp. 36, 37).

[59] P. C. Weber, D. H. Ohlendorf, J. J. Wendoloski, and F. R. Salemme, «Structural origins of high-affinity biotin binding to streptavidin», *Science*, vol. 243, no. 4887, pp. 85–88, 1989. DOI: 10.1126/science.2911722 (cit. on p. 36).

[60] L. Almonte, E. Lopez-Elvira, and A. Baró, «Surface-charge differentiation of streptavidin and avidin by atomic force microscopy–force spectroscopy», *ChemPhysChem*, vol. 15, pp. 2768–2773, 2014. DOI: 10.1002/cphc.201402234 (cit. on p. 37).

[61] A. Saftics, A. Prósz, B. Türk, B. Péter, S. Kurunczi, and R. Horvath, «In situ viscoelastic properties and chain conformations of heavily hydrated carboxymethyl dextran layers: A comparative study using owls and qcm-i chips coated with waveguide material», *Scientific Reports*, vol. 8, p. 11 840, 2018. DOI: 10.1038/s41598-018-30201-6 (cit. on pp. 48–51).

[62] H. Yu, C. Eggleston, J. Chen, W. Wang, Q. Dai, and J. Tang, «Optical waveguide lightmode spectroscopy (owls) as a sensor for thin film and quantum dot corrosion», *Sensors*, vol. 12, pp. 17 330–42, 2012. DOI: 10.3390/s121217330 (cit. on p. 49).

[63] M. Martin, M.-B. Saab, T. Cloitre, E. Estephan, R. Legros, F. Cuisinier, L. Zimányi, and C. Gergely, «A multitechnique study of bacteriorhodopsin's photonics towards new optical devices», vol. 6991, p. 69 910, 2008. DOI: 10.1117/12.781016 (cit. on p. 49).

[64] R. Richter, K. Rodenhausen, N. Eisele, and M. Schubert, «Coupling spectroscopic ellipsometry and quartz crystal microbalance to study organic films at the solid–liquid interface», in *Springer Series in Surface Sciences*. 2018, pp. 391–417. DOI: 10.1007/978-3-319-75895-4_17 (cit. on p. 49).

[65] R. Konradi, M. Textor, and E. Reimhult, «Using complementary acoustic and optical techniques for quantitative monitoring of biomolecular adsorption at interfaces», *Biosensors*, vol. 2, pp. 341–376, 2012. DOI: 10.3390/bios2040341 (cit. on p. 49).

[66] J. Malmström, H. Agheli, P. Kingshott, and D. S. Sutherland, «Viscoelastic modeling of highly hydrated laminin layers at homogeneous and nanostructured surfaces: quantification of protein layer properties using qcm-d and spr», *Langmuir*, vol. 23, no. 19, pp. 9760–9768, 2007. DOI: 10.1021/la701233y (cit. on p. 49).

[67] *What is qcm-d?*, Accessed on 09.08.2022. [Online]. Available: https://www.biolinscientific.com/blog/what-is-qcmd#:~:text=The%5C%20fundamental%5C%20working%5C%20principle%5C%20of,on%5C%20its%5C%20mass%5C%20(thickness) (cit. on p. 50).

[68] M. Müller, X. Yan, S. Lee, S. Perry, and N. Spencer, «Lubrication properties of a brushlike copolymer as a function of the amount of solvent absorbed within the brush», *Macromolecules*, vol. 38, pp. 5706–5713, 2005. DOI: 10.1021/ma0501545 (cit. on pp. 50, 55).

[69] M. Rodahl, M. Jonson, and B. Kasemo, «Viscoelastic acoustic response of layered polymer films at fluid-solid interfaces: Continuum mechanics approach», *Phys. Scr.*, vol. 59, p. 391, 1998. DOI: 10.1238/Physica.Regular.059a00391 (cit. on p. 51).

[70] E. Williams, A. Davydov, A. Motayed, S. Sundaresan, P. Bocchini, L. Richter, G. Stan, K. Steffens, R. Zangmeister, J. Schreifels, and M. Rao, «Immobilization of streptavidin on 4h-sic for biosensor development», *Applied Surface Science*, vol. 258, pp. 6056–6063, 2012. DOI: 10.1016/j.apsusc.2012.02.137 (cit. on p. 54).

[71] M. Heuberger, T. Drobek, and J. Vörös, «About the role of water in surface-grafted poly(ethylene glycol) layers», *Langmuir : the ACS journal of surfaces and colloids*, vol. 20, pp. 9445–8, 2004. DOI: 10.1021/la048384k (cit. on p. 55).